[Supplementary Material]

Water uncertainty, ritual predictability and agricultural canals at Chaco Canyon, New Mexico

Vernon L. Scarborough[1,*], Samantha G. Fladd[1,2], Nicholas P. Dunning[3], Stephen Plog[4], Lewis A. Owen[5], Christopher Carr[3], Kenneth B. Tankersley[1,5], Jon-Paul McCool[3,6], Adam S. Watson[7], Elizabeth A. Haussner[8], Brooke Crowley[1,5], Katelyn J. Bishop[9], David L. Lentz[10] & R. Gwinn Vivian[11]

[1] *Department of Anthropology, University of Cincinnati, 481 Braunstein Hall, Cincinnati, OH 45221, USA*

[2] *School of Anthropology, University of Arizona, 1009 E. South Campus Drive, Tucson, AZ 85721, USA*

[3] *Department of Geography and GIS, University of Cincinnati, 401 Braunstein Hall, Cincinnati, OH 45221, USA*

[4] *Department of Anthropology, University of Virginia, 1702 University Avenue, 100 Brooks Hall, Charlottesville, VA 22903, USA*

[5] *Department of Geology, University of Cincinnati, 500 Geology Physics Building, Cincinnati, OH 45221, USA*

[6] *Department of Geography & Meteorology, Valparaiso University, Kallay-Christopher Hall, 1809 Chapel Drive, Valparaiso, IN 46383, USA*

[7] *Division of Anthropology, American Museum of Natural History, Central Park West at 79th Street, New York, NY 10024, USA*

[8] *Department of Earth and Planetary Sciences, American Museum of Natural History, Central Park West at 79th Street, New York, NY 10024, USA*

[9] *Department of Anthropology, University of California, Los Angeles, 375 Portola Plaza, 341 Haines Hall, Los Angeles, CA 90095, USA*

[10] *Department of Biological Sciences, University of Cincinnati, 614 Rieveschl Hall, Cincinnati, OH 45221*

[11] *Department of Archaeology, Arizona State Museum, 1013 E. University Boulevard, Tucson, AZ 85721, USA*

[*] *Author for correspondence (Email: scarbovl@ucmail.uc.edu)*

Supplementary Materials 1: Optically Stimulated Luminescence Dating

Background

The 17 optically stimulated luminescence (OSL) dating samples/ages that are presented in the paper are part of a larger program of numerical dating that we undertook during the summers of 2014 and 2015 in Chaco Canyon. Thirty-six OSL samples were analysed during our studies (Haussner 2016). All the samples yielded OSL ages and—with the exception of two samples, one of which is included in this study (Chaco 2014-12)—were in stratigraphic order, i.e., they were progressively younger as the elevation increased within each studied section (S3).

OSL dating determines the time elapsed since a sediment sample was last exposed to daylight (Aitken 1998). The method relies on the interaction of ionizing radiation with electrons in semi-conducting minerals within buried sediment, which results in metastable accumulation of charge. Illumination of the sediment releases the charge as a measurable emission of photons (luminescence). The methods assume that mineral grains during or immediately prior to the transport were exposed to daylight to set them to their geological zero residual level. Upon burial, day light exposure ceases and essentially the luminescence signal begins to accumulate due to the radiation arising from the decay of ambient radioisotopes that include U, Th, Rb and K, and from cosmic rays. Given that, as a first approximation, the radiation exposure (the dose rate - D_R) is constant over the timescales of interest, luminescence builds up (equivalent dose - D_E) in the minerals in proportion to the duration of burial and the concentration of the radioisotopes in the sample environment and the cosmic dose. The depositional age (A) of the sample is thus a ratio of luminescence acquired and the rate of luminescence acquisition, i.e., $A=D_E/D_R$ (Aitken 1998; Murray & Olley 2002; Singhvi & Porat 2008).

Preparation and measurement

All the OSL samples were collected in 15cm-long, 5cm-diameter steel tubes. The tubes remained sealed until opened in the Luminescence Dating Laboratory at the University of Cincinnati under safe light conditions. A 2.5cm thick layer of sediment was removed from each end of each tube to obtain sediment from the centre of the tube for processing to reduce the possibility that any sampled sediment was exposed to daylight during the sampling procedure. The sediment from the ends of each of the tubes was dried to determine the water content of each sample. The

sediment was then crushed and sent to the Activation Laboratories Limited in Ancaster, Ontario, Canada for Major Elements Fusion ICP/MS/Trace Elements analysis to determine the U, Th, and K concentrations for D_R calculations (S3).

The remaining sediment was pretreated with 10% HCl and 10% H_2O_2 to remove carbonates and organic matter, respectively. The pretreated samples were rinsed in water, dried and sieved to attract the 90–250μm particle size fraction. A sub-fraction (~20g) of sample was etched using 44% HF acid for 80 minutes to remove the outer alpha irradiated layer from quartz particles. This treatment also helps dissolves any feldspars present. Any fluorides precipitated during HF treatment were removed using concentrated HCl for 30 minutes. The quartz sample was then rinsed in distilled water and acetate, and dried. Next, a low field controlled Frantz isodynamic magnetic separator (LFC Model-2) was used to separate feldspar and magnetic minerals from quartz following the methods of Porat (2006) with the forward and side slopes set at 100° and 10°, respectively, within a variable magnetic field. The quartz from samples collected in 2015 was re-sieved to obtain a narrower grain size of 90-125μm for OSL measurement.

An automated Riso OSL reader model TL-DA-20 was used for OSL measurements and irradiation. Aliquots, containing approximately several hundred grains of the samples, were mounted onto ~10mm-diameter stainless steel discs as a small central circle ~5mm in diameter. Aliquots for each sample were first checked for feldspar contamination using infrared stimulated luminescence (IRSL) at room temperature before the main OSL measurements were undertaken (Jain & Singhvi 2001). If the aliquots did not pass the IRSL test, the samples were etched in 40% HF for another 30 minutes to remove any feldspar, followed by 10% HCl treatment and sieving again. Samples that passed the IRSL test were used for OSL dating. Aliquots of samples were illuminated with blue LEDs stimulating at a wavelength of 470nm (blue light stimulated luminescence – BLSL). The detection optics comprised Hoya U-340 and Schott BG-39 colour glass filters coupled to an EMI 9235 QA photomultiplier tube. The samples were irradiated using a $^{90}Sr/^{90}Y$ beta source. The single aliquot regeneration (SAR) method (Murray & Wintle 2000, 2003) was used to determine the D_E for age estimation. Only aliquots that satisfy the criterion of a recycling ratio not more than 10% were used in determining D_E. A preheat of $240°C$ for 10 seconds was used and the OSL signal was recorded for 40 seconds at $125°C$. OSL sensitivity of the samples had a high signal to noise ratio. Dose recovery tests (Wintle & Murray 2006)

indicate that a laboratory dose of 10.9 Gy could be recovered to within 10% by the SAR protocol, suggesting that the protocol was appropriate.

Results

The table in S3 presents the radioisotope, water content, and cosmic dose, D_R, D_E, and OSL age for the samples. Dose rate calculations follow the details highlighted in the footnotes of the table and confirmed using the Dose Rate and Age Calculator (DRAC) of Duncan *et al.* (2015). Dose rates for all samples are very similar with values between 2.4 and 3.2 Gy/ka, which is within the normal range for terrestrial sediments. However, the Th/U is somewhat high suggesting possible leaching of U with respect to Th, which might indicate that dose rates have changed over time. Natural water content was <10%, and we assumed a conservative value with a large uncertainty (10±5%) to reflect possible changes in water content over the geologic history.

The natural OSL signal for all aliquots were at least an order of magnitude greater than background signal. The shine down curves (luminescence stimulated in the lab over 40 seconds of exposure to light) for all aliquots showed fast decay patterns that confirm that the signal is the fast component of luminescence, which is dominant in quartz. This provides confidence that the sample would have likely been bleached quickly if only briefly exposed to sunlight. IRSL "shine down" curves are also used to test that there was no feldspar within the sample. Dose rate recovery tests for the samples show that they have good recovery within the uncertainty of the laboratory measurement.

The luminescence signal for samples were at least one or two orders of magnitude greater than laboratory background. Most aliquots provided good recuperation and recovery. The dose rate recovery was excellent for all samples (within 5% of assigned dose), which provides confidence in the suitability of the sediment for OSL dating. The spread of D_E was relatively large for some samples (S3), which suggests possible partial bleaching for some of the samples. This can result in an overestimate of the age. We therefore use the weighted mean value for the D_E values for the lowest 20% of the aliquots (S3). Twenty percent of the aliquots were used to provide a generous uncertainty to the ages. Ages calculated using all the aliquots are provided in S3.

References

AITKEN, M.J. 1998. *An introduction to optical dating: the dating of Quaternary sediments by the use of Photon-stimulated Luminescence*. New York: Oxford University Press.

DUNCAN, J.A., G.E. KING & G.A.T. DULLER. 2015. DTAC: Dose Rate and Age Calculator for trapped charge dating. *Quaternary Geochronology* 28: 54-61 https://doi.org/10.1016/j.quageo.2015.03.012

GRÜN, R. 1991. Age Calculation software for Riso Laboratories.

HAUSSNER, E.A. 2016. A revised Middle to Late Holocene alluvial chronology of Chaco Canyon, New Mexico. Unpublished MS dissertation, University of Cincinnati.

JAIN, M., J.H. CHOI, & P.J. THOMAS. 2008. The ultrafast OSL component in quartz: origins and implications. *Radiation Measurements* 43(2–6): 709–14. https://doi.org/10.1016/j.radmeas.2008.01.005

MURRAY, A.S., & J.M. OLLEY. 2002 Precision and accuracy in the optically stimulated luminescence dating of sedimentary quartz: a status review. *Geochronometria* 21: 11–16.

MURRAY, A.S., & A.G. WINTLE. 2000 Luminescence dating of quartz using an improved single-aliquot regenerative-dose protocol. *Radiation Measurements* 32(1): 57–73. https://doi.org/10.1016/S1350-4487(99)00253-X

— 2003. The single aliquot regenerative dose protocol: potential for improvements in reliability. *Radiation Measurements* 37(4-5): 377–81. https://doi.org/10.1016/S1350-4487(03)00053-2

PORAT, N. 2006. Use of magnetic separation for purifying quartz for luminescence dating. *Ancient TL* 24(2): 33–6.

PRESCOTT, J.R., & J.T. HUTTON. 1994. Cosmic ray contributions to dose rates for luminescence and ESR dating: large depths and long-term time variations. *Radiation Measurements* 23(2-3): 497–500. https://doi.org/10.1016/1350-4487(94)90086-8

SINGHVI, A.K., & N. PORAT. 2008. Impact of luminescence dating on geomorphological and palaeoclimate research in drylands. *Boreas* 37(4): 536–58. https://doi.org/10.1111/j.1502-3885.2008.00058.x

WINTLE, A.G., & A.S. MURRAY. 2006. A review of quartz optically stimulated luminescence characteristics and their relevance in single-aliquot regeneration dating protocols. *Radiation Measurements* 41(4): 369–91. https://doi.org/10.1016/j.radmeas.2005.11.001

Supplementary Materials 2: Coring, particle size analysis, and the fence diagram (Figure 3)

Coring

The JMC ESP Plus Sub-Soil Probe used in the field extracts 3cm diameter sediment samples from below the ground surface (Figure S2.1). Using manual force, a hallow steel shaft containing a polyethylene terephthalate plastic tube liner was driven into the ground; upon lifting the steel shaft, the encased materials held in situ within the plastic liner were extracted (Lane *et al.* 2015). Each tube is 91.6cm long allowing a maximum extension of 2.74m below surface (3 tubes or "sections"). In order to minimize infilling of the coring hole between core sections, recycled plastic lumbar boards were placed around the borders of the hole with the base of the coring machine placed on top. This resulted in a loss of 2-4cm of maximum coring depth, but preserved the dimensions of the core and minimized the erosion of upper material into lower contexts. Once sections were removed from the device, the ends of each tube were sealed and labelled to demarcate the location of the core, the section number, and the orientation of the materials (i.e., which sediment was nearer the surface). The collected cores were returned to the University of Cincinnati for analysis. Once in the laboratory, cores were divided into 10cm segments. In addition to coring, units were excavated for archaeological and geoarchaeological purposes. Profile exposures along the Chaco Wash were also cleaned and examined. Samples were collected from distinct depositional or pedogenic horizons within excavated units and exposed profiles as well as at 10cm depths from the soil cores.

Cores were taken at ca. 40 meter intervals along three parallel-trending southwest to northeast transects in the dune dam area. Additionally, coring was done at the base of Op. C01 and Op. C02 upon completion of unit excavation. Excavation units reached roughly 1-meter depths, so the latter cores provided a picture of sediments ranging from 1 to 4 meters below the ground surface. The fence diagram was derived from the "B" and "C" lines of cores and excavation exposures as identified in Figure 1 and 7 (see below).

Sieve analysis:

Approximately 50ml of sample material (disaggregated using a ceramic mortar and pestle and 50ml volume assessed by filling a small beaker) was sub-sampled from each 10cm core segment, as well as samples collected from defined stratigraphic units within profiled exposures and

excavation operations, and were used for sieve analysis. Dry sieve analysis was completed using a nested set of 8-inch diameter sieves of the following mesh sizes: 12.5mm (-3.6 ϕ), 9.51mm (-3.25 ϕ), 4.75mm (-2.25 ϕ), 1.18mm (-0.24 ϕ), 850μm (0.23 ϕ), and 600μm (0.7 ϕ). Sieve analysis of the gravel and sand fraction is based on a modification of the post-hydrometer analysis of sands in the USDA Soil Survey's method 3.2.1.2.1, and methods employed for sand sized analysis within the USGS (USGS 2000; Burt 2014). The ca. 50ml of disaggregated sample was placed in the nested sieve set on a shaker. Following shaking, each sieve size fraction was visually examined for aggregates of smaller fractions. If aggregates were identified, the sample was again disaggregated using mortar and pestle and passed through a sieve starting with the sieve size from which the aggregates were obtained. Once no aggregates were found, the mass of sample from each sieve fraction was weighed and bagged.

Laser diffraction particle size analysis:

The sub-600μm material from each sample was tested using a Beckman Coulter LS 230 Laser Diffraction Particle Size Analyzer according to the following procedure. The material was mixed using a spatula. A sub-sample was then taken ranging in mass from 0.2 to 0.5g with the mass recorded and placed in 12ml plastic vials. For each individual sample, three sub-samples were measured for processing on the LS 230. Approximately 10ml of 50g/L hexametaphosphate solution was added to each vial as a deflocculant, followed by 10-30 seconds of end over end shaking. Samples were allowed to sit overnight while covered to promote deflocculation. Samples were then run on a Beckman Coulter LS 230 by using Beckman Coulter's Autoprep Station and Variable Speed Fluid Module to allow for faster processing. Groups of nine samples were run at a time resulting in a total of 27 vials in the autoprep station with two loess standards in positions 1 and 17 to check for variation.

LS 230 Settings:

- Control Software version 3.19
- System Flush following each sample
- Auto-Dilution Enabled
- Measure background
- Pump Speed: 48
- Optical Model: Fraunhofer, PIDS included

- Repeats: 3 repeated measures for each run

Of the 116 channels measured by the LS 230 covering the range from 0.04μm to 2mm, 104 of them cover the range between 0.04μm and 600μm (channels are synonymous with 'bins' in distribution analysis; non-overlapping, consecutive intervals of a variable). Average volume percentages for each bin were determined for the 3 sub-samples of any given sample using all 9 individual readings. Bins were then summed to determine proportions of <600μm material in standard size ranges (Clay: <2μm; Silt: 2-50μm; Very Fine Sand: 50-100μm; Fine Sand: 100-250μm; Medium Sand: 250-600μm). Percentage of the whole sample for a given size range was determined using the proportionate mass of the <600μm material to total sample mass. The method of using relative proportion of <600μm material mass to the full sample mass relies on the assumption of equal average density across particle sizes (i.e. clay is not denser than sand given an equal volume mineral material). This assumption and the assumption of sphericity are also assumptions of Stoke's Law, which underlies both the Hydrometer or Pipette methods of particle size analysis (Soil Survey Staff 2014 discussion of pipette analysis and Stoke's Law in method 3.2.1.2.2).

Fence diagram:

Textural data were combined from two coring transects, lines B and C, that ran from the southwest to the northeast of our project area. Core line B starts with Op. A08 (even though it is somewhat downstream, it is included to illustrate continuity across the canyon bottom), and includes Op. C02. Core line C includes Ops. C01/C03. C line cores also make a further adjustment north to include Op. C04 and core C07. Textures are based on nomenclature from the United States Department of Agriculture's Natural Resource Conservation Service soil texture triangle (Burt 2014). Modification such as identifying a loam as a sandy loam were made where a difference of a few percent align classification to surrounding textures; or compositional percentage was significantly different than adjacent units, but that variation was not captured by nomenclature. Full data files for particle size at each location are available upon request.

Sedimentary history interpretation:

Sandstone bedrock comprises the northern limit of the Chaco Wash alluvial zone and is believed to be traceable below the surface until core C06, which terminated at an impenetrable sub-

surface obstruction and contained sandstone fragments within the tungsten steel core tip. All other cores south of C06 were taken to the maximum sampling depth indicating bedrock depth increases with distance from the North Mesa rock face.

Deposition was divided between the anthropogenic canal sediments and the natural fluvial deposits. Anthropogenic deposits were found in Vivian's A-3e profile (Figure 5), which was investigated in detail in Ops. C01/C03 (Figure 4). Additional anthropogenic sediment was found in Op. C04. Based on sediment depth variability in these deposits, and the clear linear depression following the North Mesa rock face, the variability found in core C07 is also believed to represent anthropogenic canal sediments. In contrast to these deposits are the natural depositional patterns of the Canyon. Sandy sediment can be derived from aeolian inputs (possibly from the dune to the immediate west) or short distance water transport off of sandstone bedrock of the North Mesa, as well as potentially resulting from faster fluvial deposition by past movements of Chaco Wash itself.

Much of the sandy material at the northern end of the fence diagram (Figure 3) is believed to be North Mesa runoff or aeolian deposition with canals placed on those sediments, composing intervening deposits within canal sediments or matrices capped by such sediment. Moving south along the fence diagram profile, there are significant amounts of loam at depths that are likely due to partial input from Chaco Wash as well as the input of a sand component derived from aeolian and local bedrock outwash. This lower deposit is undated, but given its presence below the canal sediments in Ops. C01/C03, it can be fairly confidently stated that it is pre-Puebloan in age. Sediments overall become finer farther south, closer to the modern position of Chaco Wash, varying between a silt loam and a clay loam. The detailed identification of these deposits was investigated in Op. C02 and studied at the exposed wash profile Op. A08. The silt loam and loam are active fluvial deposits in the lower portions of Op. C02. Figure S2.4 shows the forset beds of fairly small ripple marks in sediments of Op. C02, as seen in the profile wall (east) and in the banding at the base of the pit when this photo was taken. This depth and structure is represented as the green silt loam underlying the blue clay loam, with the dark vertic horizon shown in Figure S2.5 by cracks infilled with aeolian surface sands.

Importantly, the transition from silt loam sediment to clay loam indicates a shift from active fluvial depositional events to a very calm depositional environment. Horizontal laminations can be seen to a small extent at the base of this clay loam in Figure S2.6 in the areas

marked by red boxes. Such laminae would have destroyed the vertic shrink-swell processes through most of the unit. Deposition of such fine-grained material in horizontal laminae is similar to ponded sediments and is indicative of extremely slow moving, if not stationary, water. Critically, this unit can be constrained to between AD 400$\pm$100 (Chaco 2015-10) and AD 1860$\pm$10 (Chaco 2015-9) and may represent the active surface during the Puebloan occupation period (S3).

Implications

The distribution of sedimentary units within the canyon has two main implications for interpreting and understanding related archaeological features. First, by comparing the depositional pattern and composition of sediments within canals to that found across the canyon in definitively identified natural fluvial settings, it can be stated without a doubt that the two are definably dissimilar. Depositional patterns of sandy, loamy, or clayey sediments identified in the excavated canals are not replicated throughout the profile except for by core C07, a location believe to be a canal based on excavation in adjacent Op. C04 and the lidar derived DEM. Second, the profile shows the lateral extent of the vertic soil identified in the Op. A08 profile and the Op. C02 excavation pit. This soil shows a different morphology than current surface soils in the canyon. Such a soil with its desiccation cracks infilled with fine aeolian material indicates a wetter local surface environment than is typically considered for the canyon floor. This could be the result of a braided stream maintaining a wetter surrounding environment (Force *et al.* 2002; Hall 1977; Hall 2010), or possibly a wet basin of water accumulation as suggested in the hotly contested 'dune dam' hypothesis (for opposing points see Force *et al.* 2002 and Hall 2010). The areal extent of this soil precludes the possibility it is simply a wet depression of the former path of Chaco Wash. Instead, the area of the canyon floor from at least core B03 to the modern incised wash was a wetter environment than the canyon surface in the area today. A key direction for future research will be in identifying the active time interval for this soil and how its environment may relate to contemporary human populations.

References

FORCE, E.R., R.G. VIVIAN, T.C. WINDES & J.S. DEAN (ED). 2002. *Relation of "Bonito" paleo-channels and base-level variations to Anasazi occupation, Chaco Canyon, New Mexico* (Arizona State Museum Archaeological Series 194). Tucson: Arizona State Museum.

HALL, S.A. 1977. Late Quaternary sediminatation and paleoecologic history of Chaco Canyon, New Mexico. *Geological Society of America Bulletin* 8: 1593–1618.

LANE, B., V.L. SCARBOROUGH & N.P. DUNNING. 2015. At the core of Tikal: terrestrial sediment sampling and water management, in D. Lentz, N.P. Dunning, & V.L. Scarborough (ed.) *Tikal: paleoecology of an ancient Maya City*: 46–58. New York: Cambridge University Press.

BURT, R (ed.). 2014. *Soil survey field and laboratory methods manual. Soil survey investigations teport No. 51, Version 2.0.* Lincoln (NE): U.S. Department of Agriculture, Natural Resources Conservation Service.

USGS. 2000. USGS East-Coast sediment analysis: procedures, database, and georeferenced displays. U.S. Geological Survey Open-File Report 00-358, prepared for U.S. Geological Survey, Department of the Interior.

Figures

Figure S2.1. In field extraction of a polyethylene terephthalate plastic lined soil cores. Top left: Hammering the core into the sediment; top right: removing core sections from the coring machine; bottom: labelled core section following extraction. Figure created by the authors.
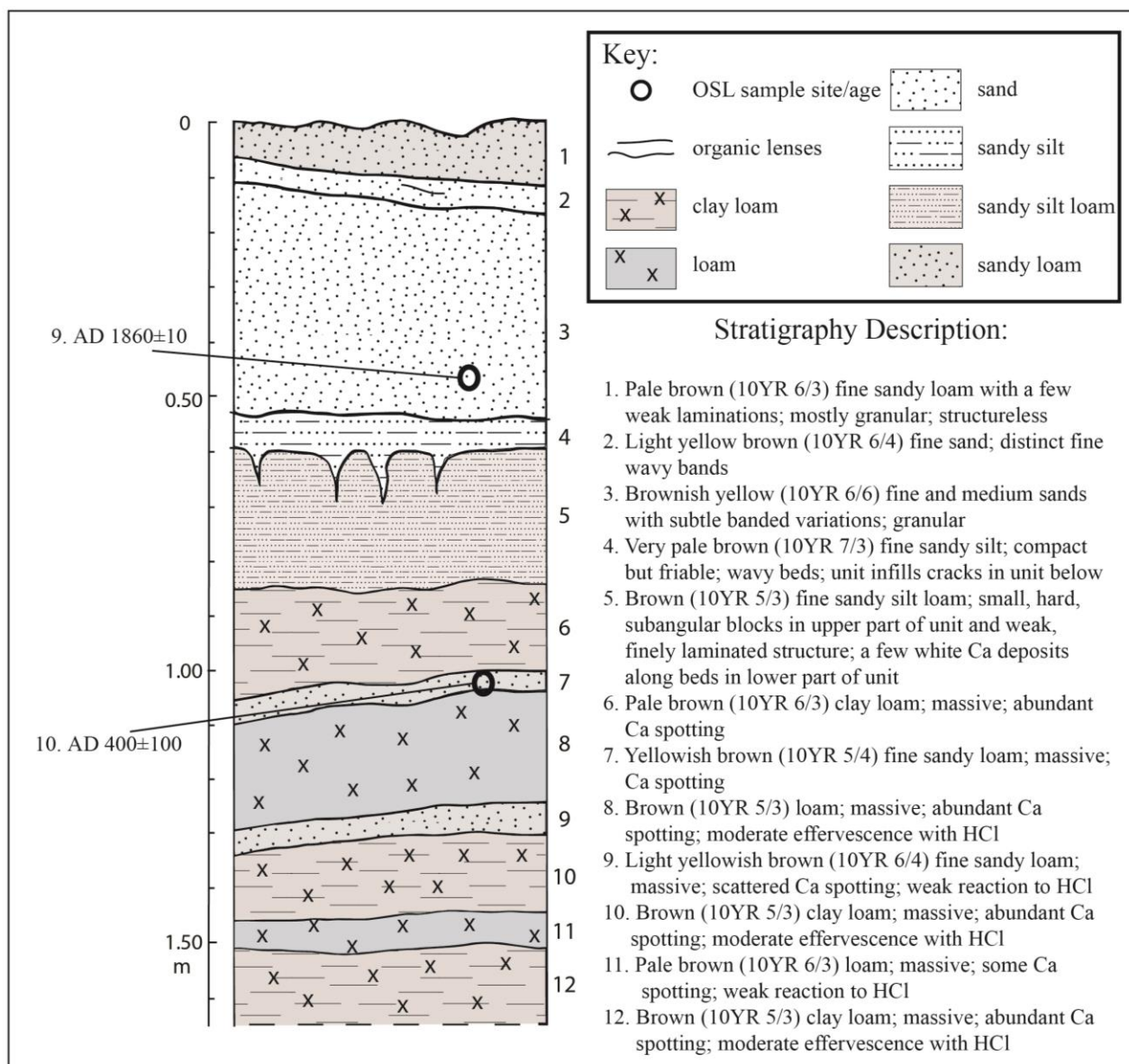
Figure S2.2. Op. A08 profile with OSL sample sites/ages. Numbers next to OSL ages refer to Chaco 2015-X in S3. Figure created by the authors.
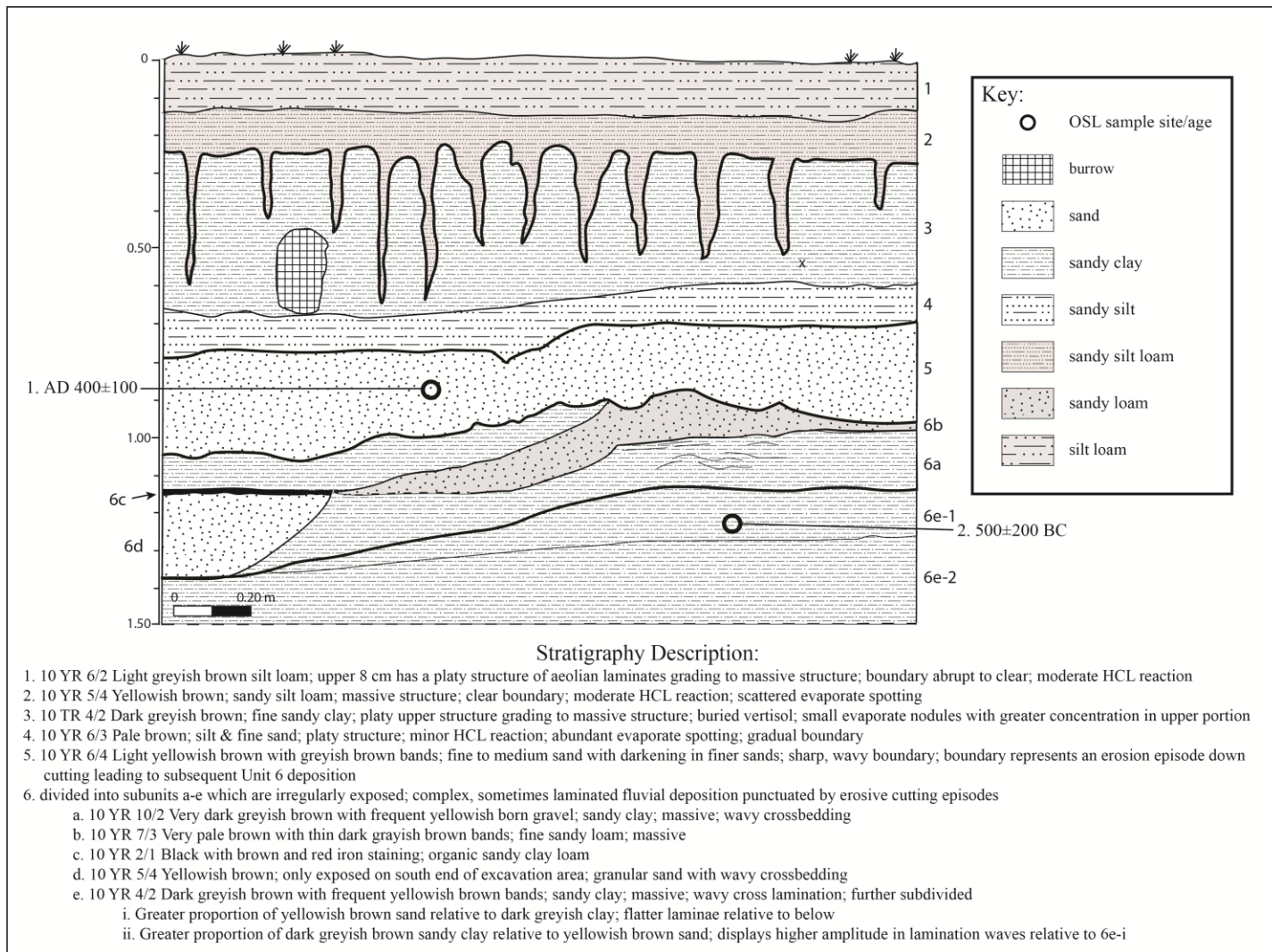
Figure S2.3. Op. C02 profile with OSL sample sites/ages. Numbers next to OSL ages refer to Chaco 2015-XX in S3. Figure created by the authors.

Figure S2.4: East profile wall and base of Op. C02 during excavation. Fluvial sediment from active deposition can be seen in the variably coloured lines at the base of the unit. These extend upward in the profile at an angle indicating they are the material on the lee side of a ripple. Figure created by the authors.

Figure S2.5: West profile of Op. C02 following excavation illustrating the relation of the lower fluvial sedimentary units (note foreset bedding in the yellow sands mid-profile) and the dark vertic soil with cracks infilled by light aeolian sediments. Figure created by the authors.

Figure S2.6: Detail of the base of the vertic soil. Red boxes indicate locations of fine horizontal lamination. These may indicate the transition from the active fluvial processes, which deposited the angled foreset bedded sands, to a calm depositional environment. The disjointed nature and lack of such laminae further up into the vertic soil is likely due to the mixing of the soil caused by vertic shrink-swell activity. Figure created by the authors.

Supplementary Materials 3: Summary of OSL dating results from extracted from sediment, sample locations, radioisotopes concentrations, moisture contents, total dose-rates, D_E estimates and optical ages.

A.

Sample number	Location (ºN/ºW)	Altitude (m asl)	Depth (cm)	U[a] (ppm)	Th[a] (ppm)	K[a] (%)	Rb[a] (ppm)	Cosmic[b, c] (Gy/ka)	Dose-rate[b, d] (Gy/ka)	n[e]	Average equivalent dose[f] (Gy)	OSL Age[f,g] (ka)	Ages in calendar years[h]
Chaco 2014-8	36.0/107.8	1925	100	2.4	8	1.7	73	0.27±0.03	2.91±0.14	48	2.62±0.02	0.9±0.04	AD 1110±40
Chaco 2014-9	36.0/107.8	1925	185	2.9	8.9	1.6	70	0.24±0.02	2.95±0.14	47	3.96±0.02	1.3±0.1	AD 700±100
Chaco 2014-10	36.0/107.8	1925	285	2.6	8.1	1.7	72	0.22±0.02	2.86±0.16	47	9.09±0.06	3.2±0.2	1200±200 BC
Chaco 2014-11	36.0/107.8	1925	320	2.9	9.9	1.8	85	0.21±0.02	3.20±0.15	46	9.25±0.08	2.9±0.1	900±100 BC
Chaco 2014-12	36.0/107.8	1924	70	2.2	6.1	1.2	54	0.28±0.03	2.34±0.14	45	6.84±0.10	3.1±0.2	1100±200 BC
Chaco 2014-13	36.0/107.8	1924	85	2.2	6.3	1.4	59	0.27±0.03	2.48±0.11	47	2.35±0.04	1.0±0.04	AD 1000±40
Chaco 2014-14	36.0/107.8	1924	50	2.1	6.2	1.3	59	0.29±0.03	2.40±0.13	48	1.36±0.03	0.6±0.03	AD 1400±30
Chaco 2015-15	36.0/107.8	1924	75	2.2	6.6	1.3	60	0.28±0.03	2.42±0.16	40	2.10±0.04	0.9±0.1	AD 1100±100
Chaco 2015-1	36.1/108.0	1859	87	2.1	6.1	1.6	70	0.27±0.03	2.62±0.16	24	4.23±0.05	1.6±0.1	AD 400±100
Chaco 2015-2	36.1/108.0	1859	122	2.4	7.4	1.8	76	0.26±0.03	2.99±0.19	23	7.38±0.07	2.5±0.2	500±200 BC
Chaco 2015-9	36.1/108.0	1854	50	1.5	4.7	2.1	74	0.28±0.03	2.93±0.20	22	0.44±0.02	0.2±0.01	AD 1860±10
Chaco 2015-10	36.1/108.0	1854	106	2.9	7.9	1.4	60	0.26±0.03	2.74±0.16	24	4.32±0.05	1.6±0.1	AD 400±100

Sample													
Chaco 2015-15	36.1/108.0	1860	117	1.9	5.7	1.7	62	0.26±0.03	2.61±0.17	24	2.85±0.04	1.1±0.1	AD 900±100
Chaco 2015-16	36.1/108.0	1860	69	1.8	5.1	1.6	60	0.28±0.03	2.54±0.16	24	2.84±0.05	1.1±0.1	AD 900±100
Chaco 2015-17	36.1/108.0	1860	28	2	5.3	1.6	61	0.29±0.03	2.67±0.17	23	2.61±0.05	1.0±0.06	AD 1000±100
Chaco 2015-20	36.1/108.0	1860	68	1.8	5.8	1.7	61	0.27±0.03	2.68±0.17	24	3.79±0.06	1.4±0.1	AD 600±100
Chaco 2015-21	36.1/108.0	1860	90	2.5	6.2	1.4	53	0.27±0.03	2.59±0.16	24	14.02±0.20	5.4±0.3	3400±300 BC

[a] Elemental concentrations from NAA of whole sediment measured at Activation Laboratories Limited Ancaster, Ontario Canada. Uncertainty taken as ±10%.

[b] Estimated fractional day water content for whole sediment is taken as 10% and with an uncertainty of ±5%.

[c] Estimated contribution to dose-rate from cosmic rays calculated according to Prescott and Hutton (1994). Uncertainty taken as ±10%.

[d] Total dose-rate from beta, gamma and cosmic components. Beta attenuation factors for U, Th and K compositions incorporating grain size factors from Mejdahl (1979). Beta attenuation factor for Rb is taken as 0.75 (cf. Adamiec and Aitken 1998). Factors utilized to convert elemental concentrations to beta and gamma dose-rates from Adamiec and Aitken (1998) and beta and gamma components attenuated for moisture content.

[e] Number of replicated equivalent dose (D_E) successfully measured determined from replicated single-aliquot regenerative-dose method (SAR; Murray and Wintle, 2000). These are based on recuperation error of < 10%.

[f] Weighted average equivalent dose (D_E) of the lower 20% of aliquots. The uncertainty includes an uncertainty from beta source estimated of ±5%.

<superscript>g</superscript> Uncertainty incorporate all random and systematic errors, including dose rates errors and uncertainty for the D_E.

<superscript>h</superscript> Calendar ages are given from year of sample measurement and rounded to the nearest decade for the last thousand years and nearest century for before AD 1000.

References

ADAMIEC, G., & M. AITKEN. 1998. Dose-rate conversion factors: update. *Ancient TL* 16: 37–50.

MEJDAHL, V. 1979. Thermoluminescence dating: beta-dose attenuation in quartz grains. *Archaeometry* 21: 61–72. https://doi.org/10.1111/j.1475-4754.1979.tb00241.x

MURRAY, A.S., & A.G. WINTLE. 2000 Luminescence dating of quartz using an improved single-aliquot regenerative-dose protocol. *Radiation Measurements* 32(1): 57–73. https://doi.org/10.1016/S1350-4487(99)00253-X

Supplementary Materials 4: Summary of AMS dating results from radiocarbon samples (Tankersley *et al.* 2017: Table 3).

Field Specimen Number	Lab Number UCIAMS[1]	Composition	¹⁴C Age BP (1 ☐☐)	Calibrated Age BP (2 ☐)[2]	Probability Distribution	Cultural Stage
DD-88	167241	*Sambucus* sp. Charcoal	170±20	0–31 138–157 165–222 258–285	0.197 0.112 0.505 0.186	Historic Navajo
DD-88	167242	*Sambucus* sp. Charcoal	170±20	0–31 138–157 165–222 258–285	0.197 0.112 0.505 0.186	Historic Navajo
DD-96	167245	Hardwood Charcoal	180±20	0–23 142–219 265–286	0.190 0.619 0.192	Historic Navajo
DD-97	167246	*Sambucus* sp. Charcoal	185±20	0–21 143–217 266–287	0.190 0.609 0.201	Historic Navajo

DD-93	167244	*Sambucus* sp. Charcoal	200±20	146–189	0.484	Historic Navajo
				193–213	0.086	
				268–296	0.267	
DD-173	167250	Hardwood Charcoal	970±25	796–875	0.595	Pueblo II
				892–933	0.405	
DD-90	167243	Hardwood Charcoal	985±20	800–813	0.058	Pueblo II
				826–865	0.263	
				901–939	0.665	
				946–953	0.013	
DD-109	167249	*Populus* sp. Charcoal	1245±20	1086–1112	0.057	Pueblo I
				1122–1159	0.078	
				1172–1266	0.866	
DD-98	167247	*Juniperus* sp. Charcoal	1690±20	1545–1624	0.926	Basketmaker II
				1671–1690	0.074	

1.   University of California, Irvine.

2.   Stuiver *et al.* (2017)

References

STUIVER, M., P.J. REIMER, AND R.W. REIMER. 2017. CALIB 7.1 [WWW program] at http://calib.org.

TANKERSLEY, K.B., L.A. OWEN, N.P. DUNNING, S.G. FLADD, K.J. BISHOP, D.L. LENTZ & V. SLOTTEN. 2017. Micro-flotation removal of coal contaminants from archaeological radiocarbon samples from Chaco Canyon, New Mexico, USA. *Journal of Archaeological Science Reports* 12: 66–73. https://doi.org/10.1016/j.jasrep.2017.01.029

Supplementary Materials 5: Provenance analysis of fluvial deposits from an Ancestral Puebloan water management feature in Chaco Canyon, New Mexico using energy dispersive X-ray fluorescence spectrometry (ED-XRF).

Introduction

For more than 100 years, archaeologists have used the mineralogical and elemental composition of materials recovered from archaeological sites to determine their provenance. See Tankersley (2007) for a discussion of the history of mineralogical and elemental provenance studies. Tankersley and Meinhart (1982), Tankersley *et al.* (1990), and Tankersley *et al.* (2011, 2015, 2016) used these techniques successfully to determine the source of raw materials to manufacture ceramic artefacts, lithic artefacts, and more recently minerals from catastrophic volcanic events. Energy Dispersive X-ray Fluorescence Spectrometry (ED-XRF) is particularly well suited to archaeological provenance studies because it is cost and time effective, requires small sample sizes, and has remarkable detection limits (e.g., 0.001% for major elements). ED-XRF can be used to obtain the complete elemental composition breakdown of sediments from the percentages of minor elements ranging to the parts per million (ppm) of trace elements (e.g., rare earths and heavy metals). Using ED-XRF analysis of fluvial deposits from a water management feature at Chaco Canyon, the elemental composition of fluvial deposits from an archaeological hydraulic feature is compared to those obtained from known water source areas.

Methods

Field Methods

Samples of fluvial deposits (~100 g) were hand-collected with a trowel in 2015 from an excavation profile of a water management feature (Ops. C01/C03), as well as Op. C02 and Op. C04. Comparative samples of modern fluvial deposits (~100 g) were collected in 2016 from several nearby North Mesa rincons (within their *tinaja* waterholes), Escavada Wash, and Chaco Wash, including its upper tributaries: the Fajada and Gallo Washes.

Laboratory Methods

Following methods described by Tankersley (2017), minor and trace element mass fractions of fluvial deposits aliquots were determined by ED-XRF. Minor elements (Na, Mg, K, C, Ti, Mn, Fe) were measured as oxides at the percent level and trace elements (Ba, Cr, Cu, Nb, Ni, Pb, Rb, Sr, V) were measured at the ppm. While values were also obtained for the elements P, As, Co, Th, and U, they were too close to the limit of detection (LOD) and the limit of quantification (LOQ) to be useful. Given the abundance of TiO_2-rich sandstone, dolomite ($CaMg(CO_3)_2$), and

vermiculite ($Mg,Fe,Al)_3((Al,Si)_4O_{10})(OH)_2.4\ H_2O$) in the Chaco Wash, Escavada Wash, and rincon drainage basins (Scott *et al.* 1984), the minor elements Ca, Mg, and Ti (measured as oxides at the percent level) were compared to fluvial deposits obtained from the excavation profile of canal features exposed in Ops. C01/C03. As such, higher concentrations of Ti should reflect a greater supply of sandstone to the sediments, whereas higher Ca and Mg concentrations should reflect a greater supply of dolomite and vermiculite.

Samples were prepared using the pressed powder pellet method described by Ingham and Starbuck (1995) and more recently by Hunt *et. al.* (2014). Approximately 10g of powdered sediment were mixed with 2 ml of Elvacite acrylic resin dissolved in a mixture of 1 liter of acetone and 200g of Elvacite powder. Aliquots were thoroughly mixed in a mortar and pestle for a period between 5 to 10min depending upon the time needed to homogenize the sample. This mixture was placed into a 40mm aluminum sample cup with a pellet-press die and compressed using a hydraulic press between 1.59—1.72 x 10^{-8} Pa for a period of 3 min. A controlled pressure release over a period between 30 and 60 sec provided a consistent analytical surface (Hunt *et al.* 2014).

Minor and trace element analysis of the powder pressed aliquots were conducted on a ThermoScientific ARL Quant'X ED-XRF analyzer. The aliquots were excited using an Rh tube with a Be end window. Following the methods described by Shackley (2011) and Hunt *et al*. (2014), dispersed X-rays were collected using a Si drift detector. The effects of Compton scatter peak were reduced by automatically adjusting the X-ray flux and current setting so the count rate and dead time of ~ 50% was achieved (Hunt *et al.* 2014).

Results

The mean percent composition of Mg is highest in sediments from the Escavada Wash (2.27 to 2.31%) and lowest in the Chaco Wash sediments, including samples from the Fajada Wash and Gallo Wash tributaries (1.00 to 1.24%) (Figure S5.1, Table S5.1). Sediments from the rincons had an intermediate mean percent composition of Mg (1.31 to 1.63%). The mean percent composition of Ca is highest in sediments from the rincons (2.94 to 4.02%) and Fajada Wash (4.92%) and lowest in the Escavada Wash (1.22 to 1.23%). Sediments from the Chaco Wash (2.06%) and Gallo Wash (2.29%) had an intermediate mean percent composition of Ca. The mean percent composition of Ti is highest in sediments from the Escavada Wash (0.79 to 0.81%)

and lowest in the rincons (0.46 to 0.64%), Gallo Wash (0.44%), and Fajada Wash (0.51%) sediments. Sediments from the Chaco Wash had an intermediate mean percent composition of Ti (0.73%). The comparisons of the minor elements Mg, Ca, and Ti demonstrate that the anthropogenic sediments at Ops. C01/C03 are comparable to those obtained from the rincons, Chaco Wash, and the Escavada Wash (Figures S5.1, S5.2, and S5.3, Table S5.2).

Implications

Our chemical analysis shows high concentrations of Ca and Mg from Menefee Formation dolomite occurs in sediment samples from Chaco Wash and the adjacent rincons, but is much lower in sediments from Escavada Wash (compare Figures S5.3 and S5.4). The high concentrations of Ti in sediment samples from the Escavada Wash are likely derived from vermiculite, which is absent in the rincon sediments. Vermiculite originated from the decomposition of biotite, which occurs in the Cliff House Formation (compare Figures S5.3 and S5.4).

Conclusions

These analyses provide empirical evidence that Ancestral Puebloans had the engineering technology to build hydraulic features that were capable of controlling water over long distances from major lateral drainages in Chaco Canyon. Fluvial deposits from Chaco Wash and Escavada Wash were identified in a hydraulic feature exposed in Ops. C01/C03. The elemental isolation of Chaco Wash, Escavada Wash, and North Mesa rincon fluvial deposits associated with the canal layers indicates redirection of waters from these separate watersheds adjacent to Chaco Canyon. To be conservative in our interpretations, we do not recognize the elemental differences between the North Mesa rincon and Chaco Wash fluvial deposits in our main analysis. While these sources can potentially be teased apart, their signatures are more similar to one another than to the Escavada Wash. The topography and hydraulic features (S7) show that Ancestral Puebloan canals were capable of drawing water from both the Chaco Wash and Escavada Wash depending upon the seasonal volume of water.

References

HUNT, A.M., D.K. DVORACEK, M.D. GLASCOCK & R.J. SPEAKMAN. 2014. Major, minor, and trace element mass fractions determined using ED-XRF, WE-XRF, and INAA for five certified clay reference materials: NCS DC 60102-60105; NCS DC 61101 (GBW 03101A, 03102A, 03103, and 03115). *Journal of Radiational Chemistry.* doi:10.1007/s10967-01403266-z

INGHAM, M.N., & P.H. STARBUCK. 1995. Investigation of the suitability of Elvacite, used as a liquid binder, for the analysis of pressed powder samples by X-ray Flouresence Spectrometry. British Geological Survey, Analytical Geochemistry Series, Technical Report WI/94/5.

SCOTT, G.R., R.B. O'SULLIVAN & D.L. WEIDE. 1984. *Geological map of the Chaco Culture National Historic Park, northwestern New Mexico*. Reston, VA: United States Geological Survey.

SHACKLEY, M.S. 2011. X-ray Fluoresence Spectrometry (XRF) in geoarchaeology. New York (NY): Springer Press. https://doi.org/10.1007/978-1-4419-6886-9

TANKERSLEY, K.B. 2007. Introduction, in T. Wilson (ed.) *Arrowpoints, spearheads, and knives of prehistoric times*: vii–ix. New York (NY): Sky Horse Publishers Press.

TANKERSLEY, K.B., & J. MEINHART. 1982. Physical and structural properties of ceramic materials utilized by a Fort Ancient group. *Midcontinental Journal of Archaeology* 7(2): 225–43.

TANKERSLEY, K.B., C. MUNSON, P. MUNSON, N. SHAFFER & R.K. LIENIGER. 1990. The mineralogy of Wyandotte Cave Aragonite, Indiana, and its archaeological significance, in N.P. Lasca & J. Donahue (ed.) *Archaeological geology of North America, Geological Society of America, Boulder, Centennial Special Vol. 4*, 219–230. Boulder (CO): Geological Society of North America. https://doi.org/10.1130/DNAG-CENT-v4.219

TANKERSLEY, K.B., V.L. SCARBOROUGH, N. DUNNING, W. HUFF, B. MAYNARD & T.L. GERKE. 2011. Evidence for volcanic ash fall in the Maya Lowlands from a reservoir at Tikal, Guatemala. *Journal of Archaeological Science* 38(11): 2925–38. https://doi.org/10.1016/j.jas.2011.05.025

TANKERSLEY, K.B., N.P. DUNNING, V.L. SCARBOROUGH, W.D. HUFF, D. LENTZ & C. CARR. 2016. Catastrophic volcanism and its implication for agriculture in the Maya Lowlands. *Journal of Archaeological Science: Reports* 5: 465–70. https://doi.org/10.1016/j.jasrep.2015.12.019
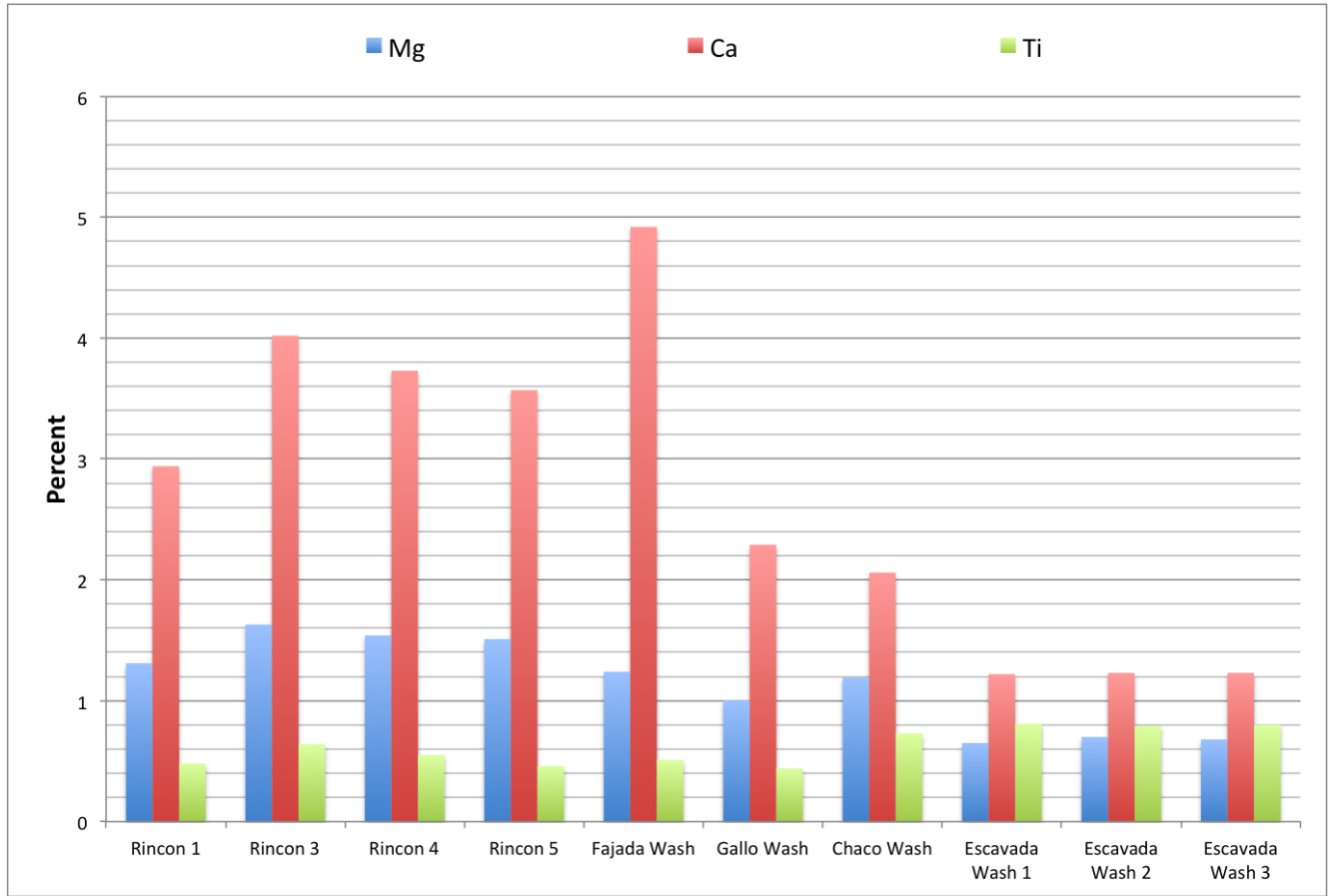
Figures:

Figure S5.1. ED-XRF analysis of the control fluvial deposit samples. The control samples are from Chaco Canyon—Chaco Wash at the trail crossing of the Peñasco Blanco trail, Escavada Wash, and North Mesa rincons—and from the Gallo and Fajada Washes just outside the Park. Figure created by the authors.
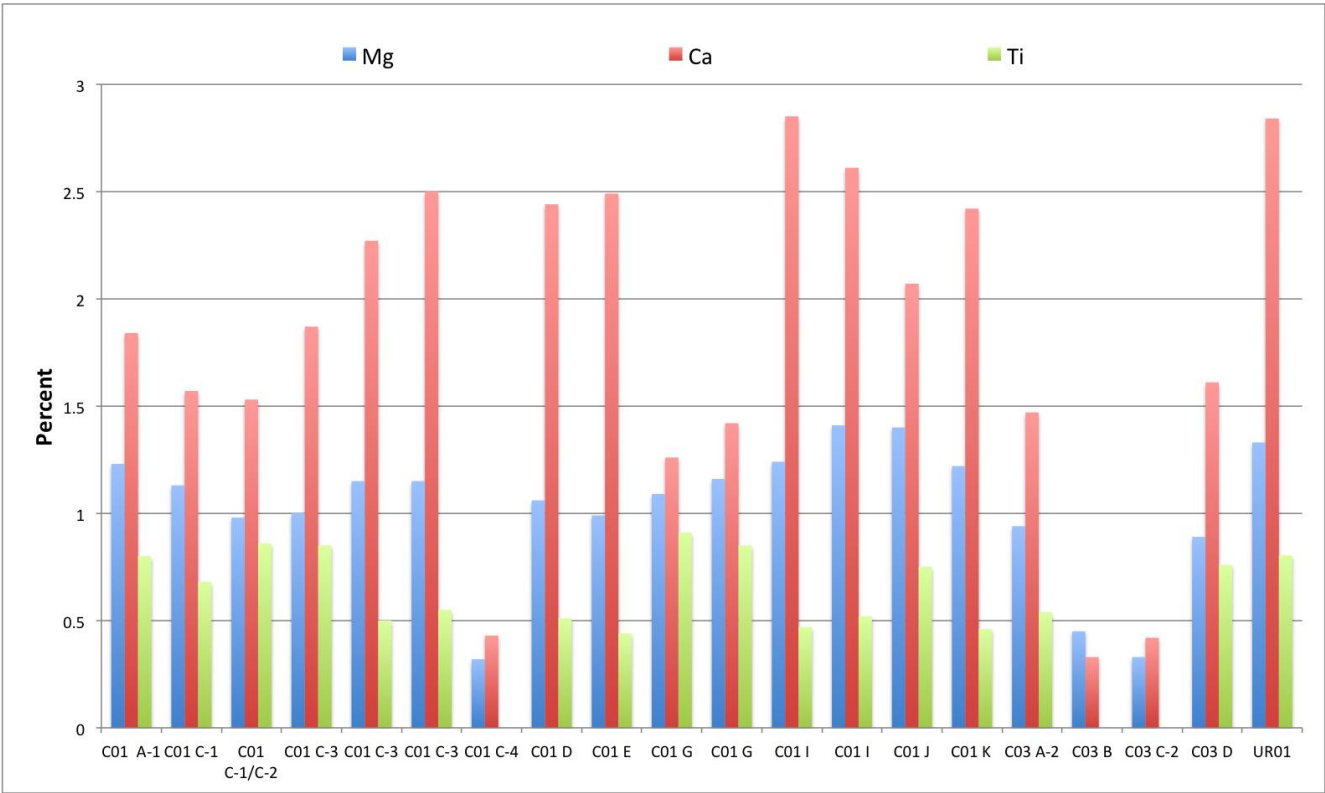
Figure S5.2. ED-XRF analysis of the archaeological fluvial deposit samples from Ops. C01/C03.
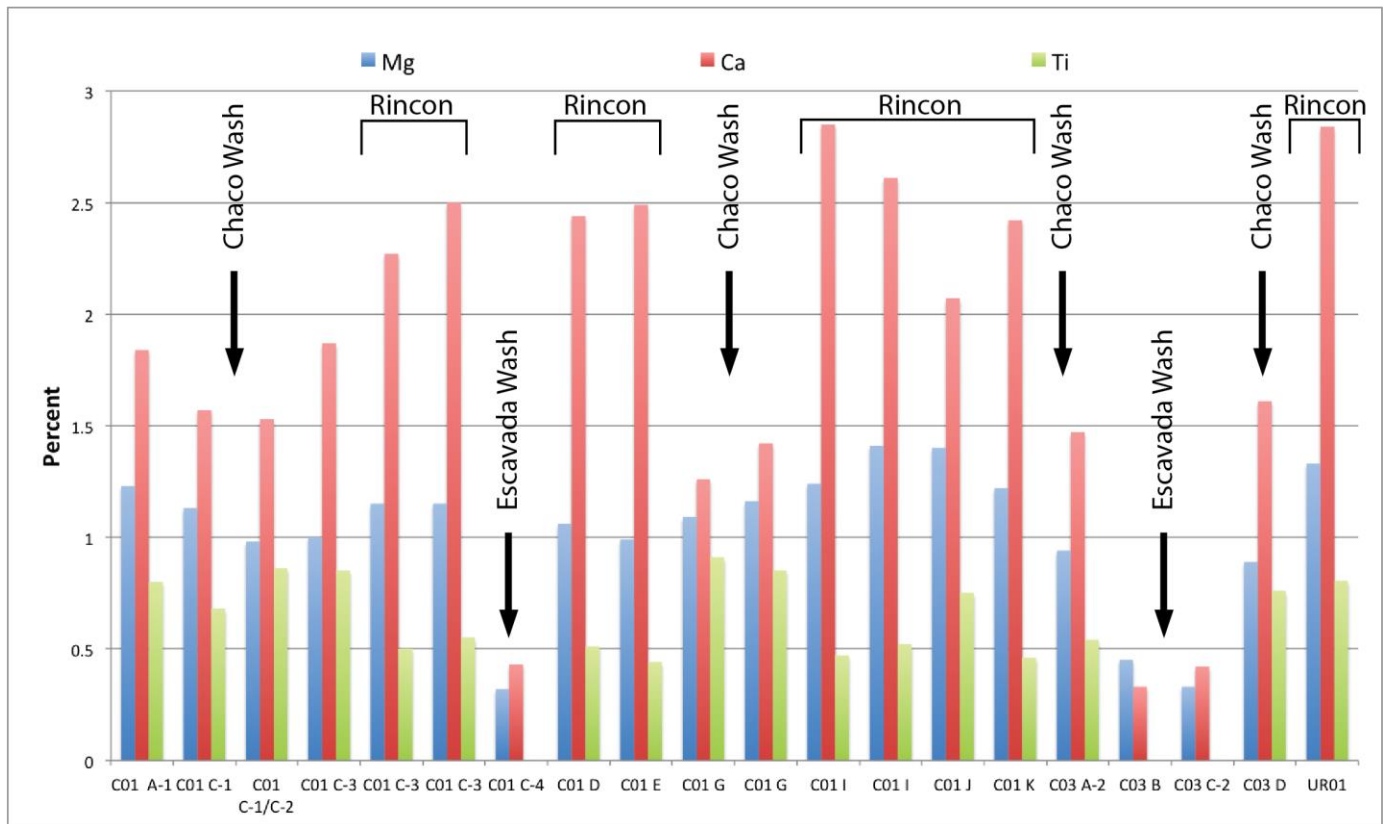Figure created by the authors.

Figure S5.3. Provenance of the archaeological fluvial deposit samples from Ops. C01/C03 based on ED-XRF analysis. Compare with Figures S5.1 and S5.2. Figure created by the authors.
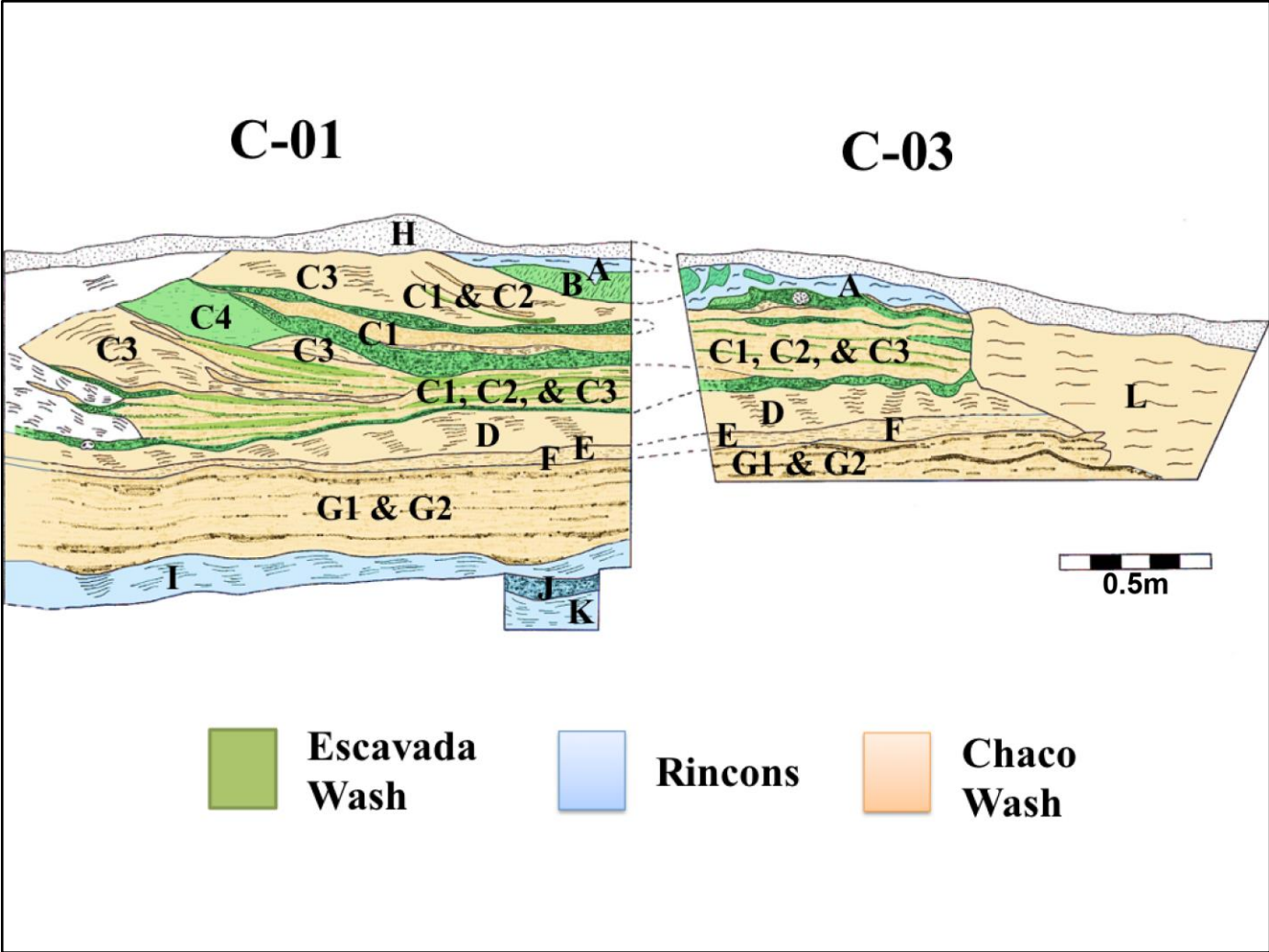
Figure S5.4. Provenance of the archaeological fluvial deposits exposed in Ops. C01/C03 based on ED-XRF analysis. Compare with Figure S5.3. Figure created by the authors.

Table S5.1: ED-XRF analysis of control fluvial deposits samples collected from water sources at Chaco Canyon. The percent minor element values represent an average of three aliquots.

Sample ID	Location Description	Mg (%)	Ca (%)	Ti (%)
Rincon 3	Rincon 3N	1.63	4.02	0.64
Rincon 4	Rincon 4N	1.54	3.73	0.55
Rincon 5	Rincon 5N	1.51	3.57	0.46
Rincon 1	Rincon 1N	1.31	2.94	0.48
Chaco F	Chaco Wash at Fajada Wash	1.24	4.92	0.51
Chaco 1	Chaco Wash at Peñasco Trail	1.19	2.06	0.73
Chaco G	Chaco Wash at Gallo Wash	1.00	2.29	0.44
Escavada 2	Escavada Wash #2	0.70	1.23	0.79
Escavada 3	Escavada Wash #3	0.68	1.23	0.80
Escavada 1	Escavada Wash #1	0.65	1.22	0.81

Table S5.2: ED-XRF analysis of control fluvial deposits samples from Ops C01/C03. The percent minor element values represent an average of three aliquots.

Sub-Op[1] Identification	Mg (%)	Ca (%)	Ti (%)
C01 I	1.41	2.61	0.52
C01 J	1.40	2.07	0.75
C01 I	1.24	2.85	0.47
C01 K	1.22	2.42	0.46
C01 G	1.16	1.42	0.85
C01 C-3	1.15	2.50	0.55
C03 C-1	1.13	1.57	0.68
C01 G	1.09	1.26	0.91
C01 D	1.06	2.44	0.51
C01 F	0.99	2.49	0.44
C03 L	0.94	1.47	0.54
C03 D	0.89	1.61	0.76
C03 B	0.45	0.33	0.00
C03 C-2	0.33	0.42	0.00
C01 C-4	0.32	0.43	0.00

1. The first designation refers to the sub-op and the second to the soil unit.

Supplementary Materials 5: Strontium Isotope Analyses

Background

Strontium isotope ratios ($^{87}Sr/^{86}Sr$) have been applied in a wide variety of geoscience studies including chronostatigraphy of marine sediments, petrology of igneous rocks, cation provenance and mobility, and quantitative models of chemical weathering. More recently the use of $^{87}Sr/^{86}Sr$ has been extended to a wide range of applications in hydrology, forensics, archaeology, ecology, and food traceability. These applications are based on the principles that (1) $^{87}Sr/^{86}Sr$ in natural materials, including animal and plant tissues, reflects the sources of strontium available during their formation, and (2) in most natural systems, the primary sources of strontium derive from surface geology (reviewed in Bentley 2006). As rocks weather, they release strontium into water

and soils, which is subsequently taken up by plants and animals. Whereas ^{86}Sr is a stable isotope, ^{87}Sr is produced by the decay of ^{87}R. Thus, the proportion of ^{87}Sr to ^{86}Sr varies with lithology and rock age, and ranges from ca. 0.7 to 0.8 in most settings (reviewed in Åberg 1995; Capo *et al.* 1998). Typical ^{87}Sr/^{86}Sr for mafic basalts is 0.702-0.705 (reflecting the Earth's mantle). Continental crustal rocks, such as granites, have higher ratios, around 0.716-0.720. Carbonates form in equilibrium with seawater, and therefore have ^{87}Sr/^{86}Sr around 0.708 (McArthur *et al.* 2001). As a rock ages, its ^{87}Sr/^{86}Sr increases due to continued decay of ^{87}Rb and production of ^{87}Sr. Thus older rocks typically have higher ratios than younger ones, and clastic sedimentary rocks (e.g., shale) typically have higher ^{87}Sr/^{86}Sr than chemical ones because they contain older detrital material. Consequently, strontium isotopes can be used to distinguish highly mobile or immigrant individuals from local residents, imported from locally-derived goods, and origins of surface or groundwater.

Chaco Canyon, located in the San Juan Basin of the southeastern Colorado Plateau, is eroded into marine sandstones and shales belonging to the Late Cretaceous Mesa Verde group (Bryan 1954; Craigg 2001). The extent to which different members of the formation are exposed is spatially variable. For example, younger members of the Formation, including the Lewis Shale, are currently only exposed near the northern boundary of the park. Additionally, multiple Quaternary fluvial, alluvial, and aeolian deposits blanket the area/ are present in the region (Hall 1977). We would, therefore, expect to find isotopic variability in bioavailable strontium among potential water sources that may have been utilized by Chaco's inhabitants (Bataille and Bowen 2012). Indeed, isotopic variability has previously been observed in sediments and waters collected from Chaco Canyon and its tributaries (Benson *et al.* 2006, 2009).

Sample Collection, Preparation, and Measurement

Water samples were collected in summer 2015 after heavy summer rains from four locations: the Chaco and Escavada Washes, and pot holes draining two rincons on the northern rim of Chaco Canyon just east of the dune dam (Figure S6.1). All four samples were fairly turbid, and sediment remained in the collection vials until a small aliquot was extracted for strontium isotope analysis in Spring 2017. Samples were analysed on a Nu plasma High Resolution multicollector inductively coupled plasma mass spectrometer (MC-ICPMS) in the Department of Geology at the University of Illinois Urbana-Champaign. An aliquot of each water sample was passed

through a 45-μm filter and placed in a Teflon autosampler vial. Strontium concentrations were checked and each sample was individually diluted with 2–3% nitric acid to yield an ^{88}Sr intensity of 8.5–11.5 volts prior to analysis. Data were corrected using international standard NBS 987, which has an accepted ^{87}Sr/^{86}Sr ratio of 0.710255, and internal laboratory reference materials 'Coral' and 'E&A', which have accepted ^{87}Sr/^{86}Sr values of 0.70918 and 0.70804, respectively. In order to control for drift throughout the run, data were normalised using the closest bracketing NBS 987 standards (Yang 2009).

In total, sediments were collected from seven locations throughout Chaco Canyon in early August 2013 using an Environmental Soil Probe as discussed in S2 and Watson *et al.* (2014). From these seven coring locations, 16 sediment samples were analysed for strontium. One coring location was located in alluvium below the Peñasco Blanco field at the lower eastern margin of the dune dam, and samples from this core will be discussed here. The core (called A00) was collected in three segments. Each is described in Table S6.1. Samples for strontium isotope analyses were selected from three depths in the core: 40-50cm, 90-100cm, and 209-219cm. These were processed following Benson (2010). Samples were dried and homogenized. Subsets of sample (ca. 5 g) from three depths were leached in 500mL of 1M acetic acid for 48 h with constant agitation. The leachate was then passed through 0.4- and 0.2mm membrane filters. Samples were prepared for analysis in a cleanroom at the Radiogenic Isotope Laboratory at the Massachusetts Institute of Technology. Samples were loaded onto Re filaments with H_3PO_4 and $TaCl_5$ activators, and analysed in dynamic multicollector mode on a VG Sector 54 thermal ionization mass spectrometer (TIMS). The lab reports that the ^{87}Sr/^{86}Sr of NBS 987 over the past 10 years has averaged 0.710246±0.00001, for analyses with ^{88}Sr = 3 x 10^{-11} amps, and that external reproducibility of ^{87}Sr/^{86}Sr analyses has been better than 25ppm (2 sigma). Total procedure blanks are less than 40pg.

Results

There is considerable isotopic variability in both water and sediment samples (Table S6.2). The Escavada Wash has considerably higher ^{87}Sr/^{86}Sr than the Chaco Wash; the two rincons have intermediate ratios. Sediments at 209-219 cm in the core isotopically resemble the Chaco Wash. However, ^{87}Sr/^{86}Sr decreases at shallower depths. Samples from 40-50cm and 90-100cm have considerably higher ^{87}Sr/^{86}Sr than modern Chaco Wash water, suggesting a different source.

Discussion and Implications

Numerous researchers have previously used strontium isotopes to identify the sources of goods, such as corn, wood, or animal prey preserved in archaeological contexts at Chaco Canyon (e.g., English *et al.* 2001; Reynolds *et al.* 2005; Benson *et al.* 2006, 2009; Benson 2010; Grimstead *et al*. 2015, 2016). Unfortunately, geologic, and therefore isotopic similarities among many of the potential source areas (e.g., Chuska Mountains, San Pedro Mountains, La Plata Mountains, San Mateo Mountains, Tohatchi Flats, and the Chaco Canyon itself) have caused researchers to question the utility of this geochemical tool for sourcing goods in the south-eastern Colorado Plateau (e.g., Drake *et al.* 2014).

To the best of our knowledge, our study is the first use of ^{87}Sr/^{86}Sr to distinguish potential water and sediment sources in Chaco Canyon. Benson and colleagues (2003, 2006) did analyse sediment samples from the valley floor and side canyons at Chaco Canyon, focusing on relatively shallow samples (<85cm from the sediment surface). Overall, ^{87}Sr/^{86}Sr for sediments ranged from 0.708973 to 0.709606 in the canyon valley and 0.708792 and 0.709709 in the side canyons (Figure S6.2). However, ratios were less variable among depths at any given sample site (Figure S6.2). Strontium isotopes for sediments sampled at 25-35cm, 55-65cm, and 85-95cm depth from Peñasco Blanco, the area where our sediments were cored, ranged from 0.709078 to 0.709204. These ratios are broadly consistent with those that we measured, but less variable, most likely because samples did not come from the exact same location and sediment deposition is not uniform. Benson and colleagues (2006) also analysed surface water samples from the Fajada, Gallo, and Chaco Washes, and two side tributaries several kilometres upstream from the confluence of the Chaco and Escavada Washes. They noted considerable isotopic variability among water sources that is comparable to what we report here (see Figure 21-8 in Benson *et al.* 2006). However, they did not discuss the implications of this variability on water management practices. They acknowledged the likelihood that Chaco's inhabitants practiced multiple forms of agriculture, including the construction of check dams and terraces, but only used strontium isotope data to support their prediction that most of the corncobs recovered from Chaco archaeological contexts were not grown within Chaco Canyon. For these reasons, as well as the issues with distinguishing Chaco and Chuska sources and the concerns later raised by co-authors

about the representativeness of the selected sample of corncobs (Cordell *et al.* 2008), agriculture within Chaco Wash cannot be discounted.

While our results must be viewed as preliminary, we feel they are compelling. Like Energy Dispersive X-ray Florescence Spectrometry (ED-XRF), strontium isotope data are consistent with multiple, different sources of water and sediments pooling in the dune dam area near Chaco Wash over time. The shift in $^{87}Sr/^{86}Sr$ may reflect filtering of water from the Escavada down slope towards the Chaco Wash, or possibly backfill of water derived from the Escavada behind a dune dam. Further analyses of sediments in the dune dam area, specifically in sediments identified as potential canal deposits, will likely be illuminating.

References

ÅBERG, G. 1995. The use of natural strontium isotopes as tracers in environmental studies. *Water, Air and Soil Pollution* 79(1–4): 309–22. https://doi.org/10.1007/BF01100444

BATAILLE, C.P., & G.J. BOWEN. 2012. Mapping $^{87}Sr/^{86}Sr$ variations in bedrock and water for large scale provenance studies. *Chemical Geology* 304–305: 39–52. https://doi.org/10.1016/j.chemgeo.2012.01.028

BENSON, L.V. 2010. Who provided maize to Chaco Canyon after the mid-12th-century drought? *Journal of Archaeological Science* 37(3): 621–9. https://doi.org/10.1016/j.jas.2009.10.027

BENSON, L.V., J. STEIN, H. TAYLOR, R. FRIEDMAN & T.C. WINDES. 2006. The agricultural productivity of Chaco Canyon and the source(s) of Pre-Hispanic maize found in Pueblo Bonito, in J. Staller, R. Tykot, & B. Benz (ed.) *Histories of maize: multidisciplinary approaches to the prehistory, linguistics, biogeography, domestication, and evolution of maize*: 289–314. Walnut Creek (CA): Left Coast Press.

BENSON, L.V, J.R. STEIN & H.E. TAYLOR. 2009. Possible sources of archaeological maize found in Chaco Canyon and Aztec Ruin, New Mexico. *Journal of Archaeological Science* 36(2): 387–407. https://doi.org/10.1016/j.jas.2008.09.023

BENTLEY, R.A. 2006. Strontium isotopes from the earth to the archaeological skeleton: a review. *Journal of Archaeological Method and Theory* 13: 135–87. https://doi.org/10.1007/s10816-006-9009-x

BRYAN, K. 1954. *The geology of Chaco Canyon, New Mexico in relation to the life and remains of the prehistoric peoples of Pueblo Bonito*. Washington, D.C.: Smithsonian Institution.

CAPO, R.C., B.W. STEWART & O.A. CHADWICK. 1998. Strontium isotopes as tracers of ecosystem processes: theory and methods. *Geoderma* 82: 197–225. https://doi.org/10.1016/S0016-7061(97)00102-X

CORDELL, L.S., H.W. TOLL, M.S. TOLL & T.C. WINDES. 2008. Archaeological corn from Pueblo Bonito, Chaco Canyon, New Mexico: dates, contexts, sources. *American Antiquity* 73(3): 491–511. https://doi.org/10.1017/S0002731600046837

CRAIGG, S.D. 2001. *Geologic framework of the San Juan structural basin of New Mexico, Colorado, Arizona, and Utah, with emphasis on Triassic through Tertiary rocks* (No. 1420). Reston (VA): US Geological Survey.

DRAKE, B.L., W.H. WILLS, M.I. HAMILTON & W. DORSHOW. 2014. Strontium isotopes and the reconstruction of the chaco regional system: evaluating uncertainty with Bayesian mixing models. *PLoS ONE* 9(8): e95580. https://doi.org/10.1371/journal.pone.0095580

ENGLISH N.B., J.L. BETANCOURT, J.S. DEAN & J. QUADE. 2001. Strontium isotopes reveal distant sources of architectural timber in Chaco Canyon, New Mexico. *Proceedings of the National Academy of Sciences of the United States of America* 98(21): 11890–6. https://doi.org/10.1073/pnas.211305498

HALL, S.H. 1977. Late Quaternary sedimentation and paleoecologic history of Chaco Canyon, New Mexico. *GSA Bulletin* 88(11): 1593–1618. https://doi.org/10.1130/0016-7606(1977)88<1593:LQSAPH>2.0.CO;2

GRIMSTEAD, D.N., S.M. BUCK, B.J. VIERRA & L.V. BENSON. 2015. Another possible source of archeological maize found in Chaco Canyon, NM: the Tohatchi Flats area, NM, USA. *Journal of Archaeological Science: Reports* 3: 181–7. https://doi.org/10.1016/j.jasrep.2015.06.003

GRIMSTEAD, D.N., J. QUADE & M.C. STINER. 2016. Isotopic evidence for long-distance mammal procurement, Chaco Canyon, New Mexico, USA. *Geoarchaeology* 31(5): 335–54. https://doi.org/10.1002/gea.21545

MCARTHUR, J.M., R.J. HOWARTH & T.R. BAILEY. 2001. Strontium isotope stratigraphy: LOWESS Version 3: best fit to the Marine Sr-Isotope Curve for 0–509 Ma and accompanying look-up table for deriving numerical age. *The Journal of Geology* 109: 155–70. https://doi.org/10.1086/319243

REYNOLDS, A.C., J.L. BETANCOURT, J. QUADE, P.J. PATCHET, J.S. DEAN & J. STEIN. 2005. $^{87}Sr/^{86}Sr$ sourcing of ponderosa pine used in Anasazi great house construction at Chaco Canyon,

New Mexico. *Journal of Archaeological Science* 32(7): 1061–75.
https://doi.org/10.1016/j.jas.2005.01.016

VOERKELIUS, S., G.D. LORENZ, S. RUMMEL, C.R. QUÉTEL, G. HEISS, M. BAXTER, C. BRACH-PAPA, P. DETERS-ITZELSBERGER, S. HOELZL, J. HOOGEWERFF, E. PONZEVERA, M. VAN BOCXSTAELE & H. UECKERMANN. 2010. Strontium isotopic signatures of natural mineral waters, the reference to a simple geological map and its potential for authentication of food. *Food Chemistry* 118(4): 933–40. https://doi.org/10.1016/j.foodchem.2009.04.125

WATSON, A.S., A. HOLEMAN, S. FLADD, K. BISHOP, M. CONGER & S. MORROW. 2014. Damage assessment and data recovery at 29SJ 2384, Roberts' Great House July-August 2013. Report prepared for the National Park Service, Chaco Culture National Historical Park.

YANG, L. 2009. Accurate and precise determination of isotopic ratios by MC-ICP-MS: a review. *Mass Spectrometry Reviews* 28(6): 990–1011.
https://doi.org/10.1002/mas.20251

Tables:

Table S6.1: Description of sediment core segments (from Watson *et al.* 2014). Apparent voids in the core reflect sediments drying and pulling apart within the core sleeves.

Segment	Depth within core (cm)	Description
1	0-40	Aeolian or alluvial sands
	40-75	Finer sediments, possible clay
2	95-100	Cave-in (mostly sand)
	125-145	Clay deposits
	145-165	Aeolian or alluvial sands
3	165-175	Cave-in sand
	177-181	Dark (rather than light) brown sand). Appears at a 45° angle
	181-197	Pocket of clay 8 cm thick
	204-230	Tan fine sand, similar to the layer above the clay pocket
	231-235	Dark brown clay-sand (?) followed by bands of aeolian/alluvial sand (light and dark)

Table S6.2: Strontium isotope data for waters and sediments in the vicinity of the dune dam.

Sample Type	Depth (cm)	Location Description	Collection Date	$^{87}Sr/^{86}Sr$	Uncertainty
Water		Escavada Wash just upstream from Confluence with Chaco Wash	31-Jul-15	0.71026	±0.00005
Water		Chaco Wash upstream from dune dam	23-Jul-15	0.70856	±0.00005
Water		Rincon #1	11-Aug-15	0.70933	±0.00005
Water		Rincon #2	12-Aug-15	0.70949	±0.00005
Sediment	40-50	East of dune dam	1-Aug-13	0.70968	±0.0006
Sediment	90-100	East of dune dam	1-Aug-13	0.70919	±0.0006
Sediment	209-219	East of dune dam	1-Aug-13	0.70884	±0.0004
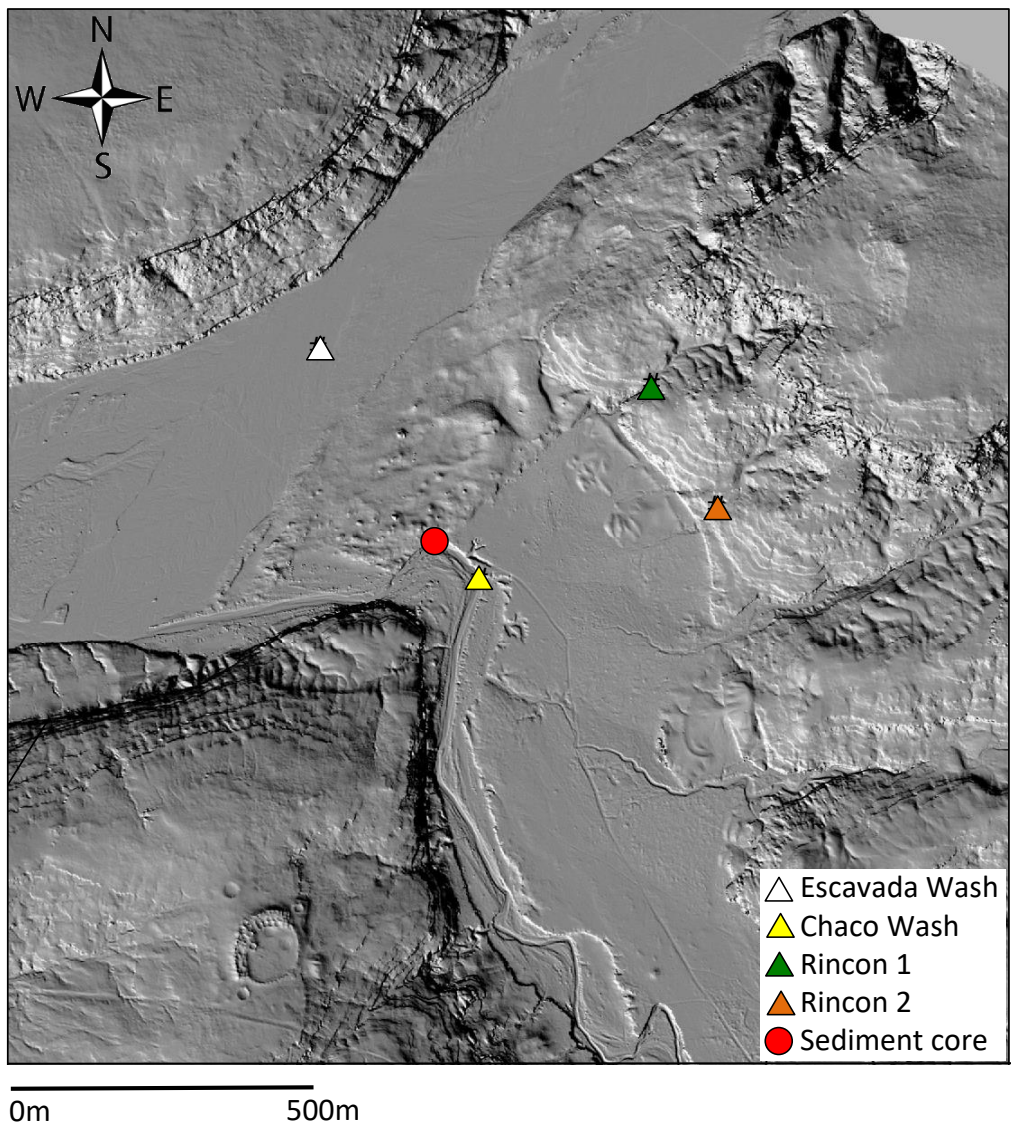
Figure S6.1: Map of the study area showing collection locations for water and sediment samples. Figure created by the authors.
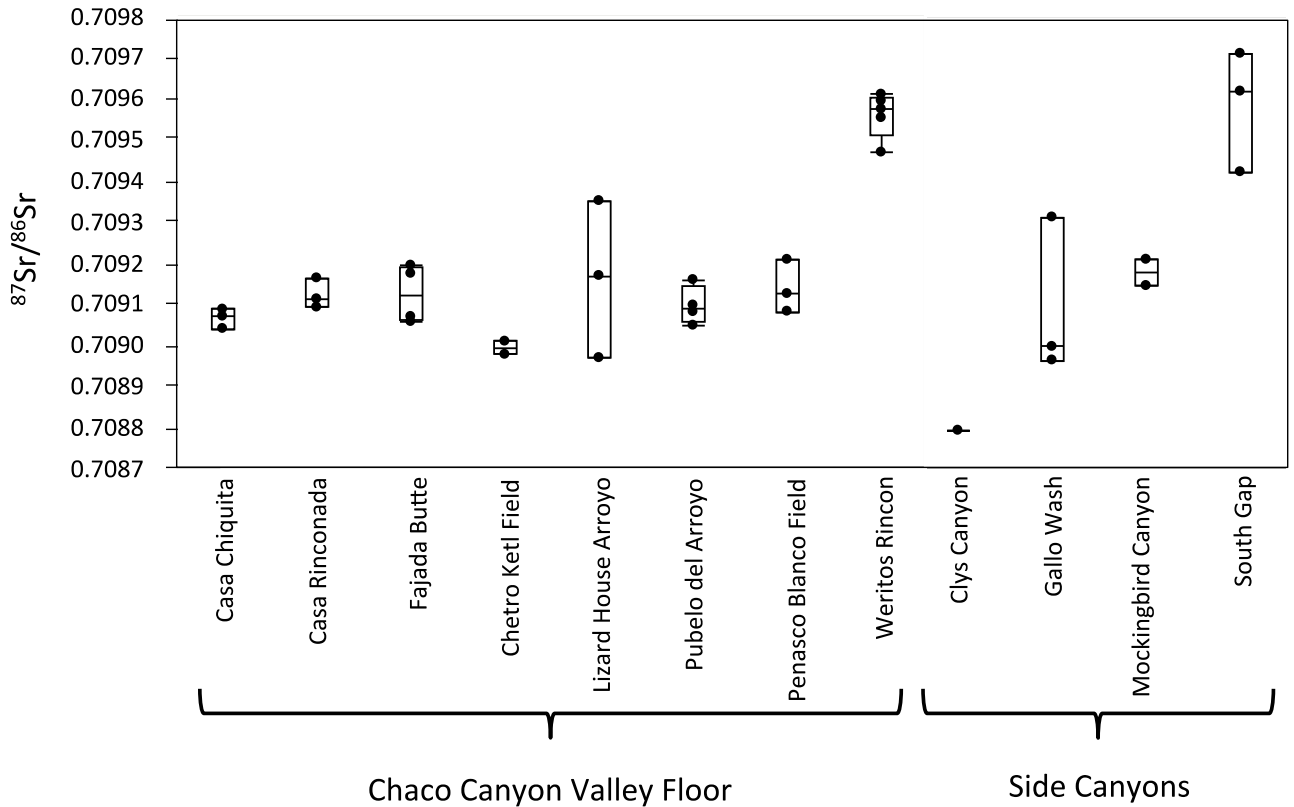
Figure S6.2: Sediment data from Chaco Canyon valley floor and side canyons (from Benson *et al.* 2006).

Supplementary Materials 7: Multiple Possible Canal Routes

Our examination of possible canal routes in the "dune dam area" was guided by the prior work of R. Gordon Vivian and R. Gwinn Vivian. We started with a landscape level analysis of the lidar-derived elevation data by way of georeferencing the Vivians' findings to the lidar. Using the lidar elevations to generate contour lines and hydrological flow lines, we positioned our Ops. C01/C03, C04, and E02 to gather additional data—primarily dates—for the features that the Vivians had previously located. The Vivians' findings are illustrated in the Gordon Vivian map of a possible Escavada Wash intake for a Chaco Canyon canal and in the reports from Gwinn Vivian's Chaco Canyon Water Control Project (CCWCP).

In all, the presence of multiple canals feeding from multiple sources shows a high degree of pre-planning of canal routes and gradients, along with continued maintenance. Further, the ongoing efforts to insure water delivery imply fertile agricultural lands in the floodplain of

Chaco Canyon (Vivian *et al*. 2006: Figure 2.2). The following sections provide additional information on Gordon and Gwinn Vivian's findings, as well as our own.

Possible Escavada Canal

Aided by the aerial photographs (e.g., Peñasco Blanco 6-4 1964), Gordon Vivian plotted observations from a group of individual water control features onto a map, which hypothesized an "Escavada Wash Water Control System" (CHCU-55430, 1971). Figure S7.1 shows the Escavada map georeferenced to the lidar. With the Escavada map georeferenced, the path of the posited canal was digitized and transferred to the lidar image. Figure 1 shows elevation contour lines derived from the lidar data (at 1856m and 185m above sea level). That the Vivian hypothesized canal roughly follows the elevations between the contour lines (lines of constant elevation) establishes the hydrologic plausibility of the canal as canals are expected to have a continuous, shallow, downward slope.

Chaco Canyon Water Control Project

Further adding to the picture of ancient Chaco use of water in the "dune dam area" is the "Chaco Canyon Water Control Project" (CCWCP). Gwinn Vivian's CCWCP looked specifically at water control features during surveys in 1970 thru 1971 (overlapping in time with the Hayes *et.al* (1981) surveys. The CCWCP findings are presented in a technical letter (Vivian 1972), on a master map (CHCU-55452 1971), and in over 130 feature forms (CHCU-85920 1971; Vivian 1971). The master map shows the locations of canals, reservoirs, sluice gates, diversion dams, pit houses, field houses, and gridded fields. A simplified version of the map is in Vivian (1972). The CCWCP located 22 water control features in the dune area. We georeferenced the CCWCP master map using the lidar image and township and range markings on the master map and then re-examined the possible canals at CCWCP sites A-3e and A-1. These two locations became our Ops. C01/C03 and C04 respectively. Using a marked up aerial photograph from Gwinn Vivian to assist with locating the A-1 to A-3e features. Figure 5 shows the CCWCP profile of feature A-3e (*pers. comm.* Gwinn Vivian, 2015).

Lidar Data

Key new information for our 2015 fieldwork was the lidar-derived elevational data for the entire canyon. These lidar data were collected in June of 2010 and released to the public shortly thereafter (Dorshow 2010). The lidar data display the elevation of the ground surface at one meter spacing within a few decimeters of vertical accuracy. We generally converted the lidar elevations into a hillshade map (e.g., Figure S7.1 and S7.2). The lidar hillshade is of high enough resolution that individual rooms in the Peñasco Blanco great house are visible (see Figure 1). The hillshade map also shows numerous linear features that may be ancient roads and/or canals. The lidar elevational data allow us to define watersheds and water flow paths, a key layer in our Geographic Information System (GIS) database. The GIS database permitted us to locate the prior research, as well as our current work, within the landscape.

The entire lidar dataset for Chaco Canyon is available to the public for download on the Open Topography website (http://www.opentopography.org/). Open Topography is a National Science Foundation supported facility at the San Diego Super Computer Center, University of California San Diego (NSF award numbers 1226353 and 1225810). The Chaco lidar files are stored under the data set name "Chaco Canyon, NM: Simulating Dynamic Hydrological Processes" and can be located using the digital object identifier—DOI: http://dx.doi.org/10.5069/G93N21B2.

Ops. C01/C03 (CCWCP A-3e)

The field form describing the A-3e excavation is part of the CCWCP (Vivian 1971). The general location of the excavation is shown on the maps in the Vivian (1972) technical letter. The specific location is identified on the large CCWCP map (CHCU 55452 1971) and on a mark-up of the c.1965 aerial photo of the area (Peñasco Blanco 6-4 1964; *pers. comm.* Gwinn Vivian). In order to build on the CCWCP work, our intention was to place our operation in close proximity to A-3e. We succeeded; the far side of our Op. C01 pit uncovered flagging tape from A-3e. Our unit is on the ridge, just upslope from A-3e.

Operation C04 (CCWCP A-1)

In February of 1971, Gwinn Vivian and Jon Haas located a possible canal in the "upper dune area." The canal most likely was positioned to collect water from the slickrock immediately

above it (CHCU-85920 1971: 31). They identified this possible canal as CCWCP project feature number A-1. Our Op. C04 is located on this possible canal.

A CCWCP sketch map roughly locates features A-1 thru A-4. The lidar hillshade map with an illumination angle of 225º (Figure 7) clearly shows a ridge which would form a canal wall running from "the dune" at the west end, across the discharge of Rincon One, to the discharge of Rincon Two at its east end. Topographic contour lines derived from the lidar elevations show an essentially level course for the ridge and associated trough between the ridge and base of the slickrock. This level-run further supports the supposition that this feature was a canal.

Using Vivian's sketch map, photographs, and the written description in the A-1 feature form, we located our Op. C04 excavation (a 1x2 meter pit) on or very close to Vivian's A-1 excavation. The excavations are similarly positioned, perpendicular to and partially on the ridge. The profile drawing of the operation is in the main text (Figure 9). The excavation yielded two OSL dates noted on the profile.

Operation E02 (Escavada map "G" and CCWCP A-13)

Op. E02 is positioned on the canal noted on the Gordon Vivian Escavada Intake map (CHCU-55430, 1971) (Figure S7.1; Figure 1) just up canal from feature "G". Feature "G" was re-examined by Gwinn Vivian as part of the CCWCP and identified as feature A-13 (CHCU-55452 1971; Vivian 1971).

Op. E02 was an expedient "cleaning" of a cut-bank in Rincon 5 made during the final day of fieldwork in 2015. We were drawn to this area because it appeared to cut across the path of the canal posited by Gordon Vivian (CHCU-55430 1971). On the lidar-derived hillshade image of the Canyon, a long linear feature is visible intersecting Rincon 5N where Op. E02 was located. On the ground, a long linear depression is clearly visible. National Park staff suggested that this linear depression was created by 19th-century wagon traffic. A prominent ridge about 80 cm in height above the depression floor and 30 cm above the adjacent valley floor runs parallel to the linear depression. The cut-bank of Rincon 5 bisected this ridge exposing stratified dipping sediment deposits resembling those exposed in the canal excavated in Ops. C01/C03 (Figures 4 and 5). A shovel was used to cut back a portion of the strata exposed in the bisected ridge (Op. E02) and the profile quickly photographed, sketched, and described (Figure 8, Figures

S7.3 and S7.4). One small carbon sample was collected, but proved too small for radiocarbon dating.

The presence of these canal-like deposits within the body of the ridge, like those of the Ops. C01/C03 canals, indicate that the canal exposure in Op. E02 was also elevated above the floor of the Chaco Wash floodplain. The elevated canal in Op. E02 is similar to the perched canal on Ops. C01/C03 (Vivian A-3e). Both may represent an aqueduct-like effort to extend the canals by controlling elevations and hence hydraulic gradients.

References

CHCU-55430. 1971. Gwinn Vivian Collection (0030)- CHCU 55430 Escavada Wash Water Control System, Plan and Sections of Escavada Wash water Control System, Plan and Sections of Escavada Wash Canal, w/ Gates, Spillway. National Park Service, Chaco Culture National Historical Park, Albuquerque, NM.

CHCU-55452. 1971. Gwinn Vivian Collection (0030)- CHCU 55452 Master Map of 1970/1971 Chaco Canyon Water Control Project (CCWCP). National Park Service, Chaco Culture National Historical Park, Albuquerque, NM.

CHCU-85920. 1971. Gwinn Vivian Collection (0030)- VA 2064 Vivian II, Chaco Canyon Water Control Project- general feature forms. National Park Service, Chaco Culture National Historical Park, Albuquerque, NM.

DORSHOW, W.B. 2010. Chaco Canyon, NM: simulating dynamic hydrological processes in archaeological contexts - Mapping Project Report. *Open Topography.* Available at: http://opentopo.sdsc.edu/datasetMetadata?otCollectionID=OT.112011.26913.1 (accessed 11 September 2017).

HAYES, A.C., D.M. BRUGGE & W.J. JUDGE. 1981. *Archeological surveys of Chaco Canyon, New Mexico* (Publications in Archeology 18A, Chaco Canyon Studies). Santa Fe (NM): National Park Service.

PEÑASCO BLANCO 6-4. 1964. Gordon Vivian Aerial Photo: Peñasco Blanco 6-4. Report Prepared for the National Park Service, Chaco Research Archive, Albuquerque, NM.

VIVIAN, R.G. 1971. Chaco Canyon Water Control Project - general feature forms. National Park Service, Chaco Culture National Historical Park, Gwinn Vivian Collection (0030)-CHCU-85920; VA 2064 Vivian II. Available at:

http://www.chacoarchive.org/bibl_database/cdi_accessions/show/20279?public=true. Accessed on August 17, 2017.

—1972. Prehistoric water conservation in Chaco Canyon. Report prepared for the National Science Foundation, Grant No. GS-3100, Washington, D.C.

VIVIAN, R.G., C.R. VAN WEST, J.S. DEAN, N.J. AKINS, M.S. TOLL & T.C. WINDES. 2006. Ecology and economy, in S.H. Lekson (ed.) *The archaeology of Chaco Canyon: an eleventh-century Pueblo regional center*: 45–65. Santa Fe (NM): School of Advanced Research Press.

Figures:
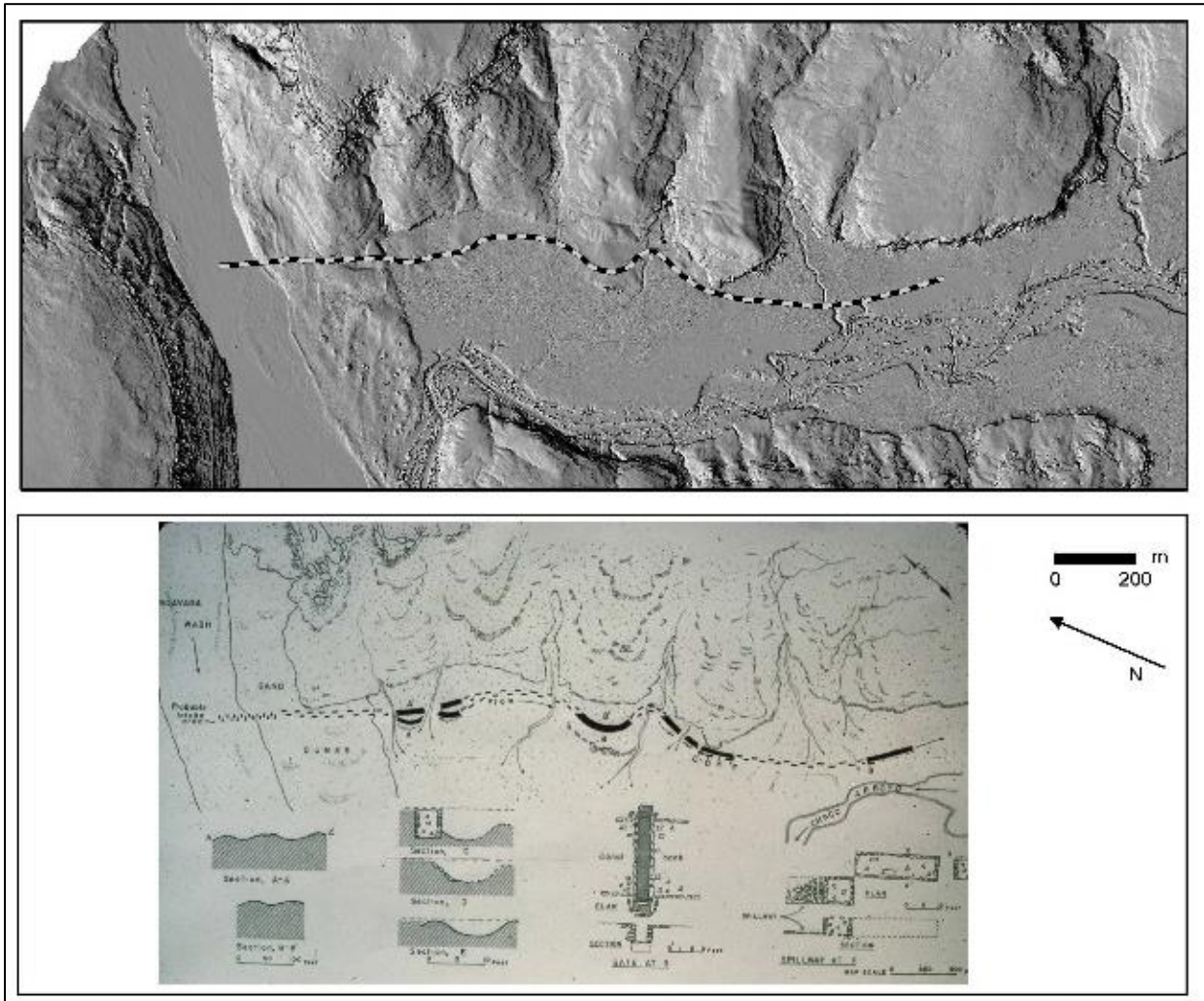
Figure S7.1: The Gordon Vivian hypothesized canal (c.1964) feeding from Escavada Wash, thru the dune and up Chaco Canyon. The Vivian map (CHCU-55430 1971; *pers. comm.* Gwinn Vivian 2015), bottom image, is aligned with the lidar-derived hillshade image above. The Vivian canal line is transposed to the lidar map. Our excavations were in the "A" section of the postulated canal. Figure created by the authors.
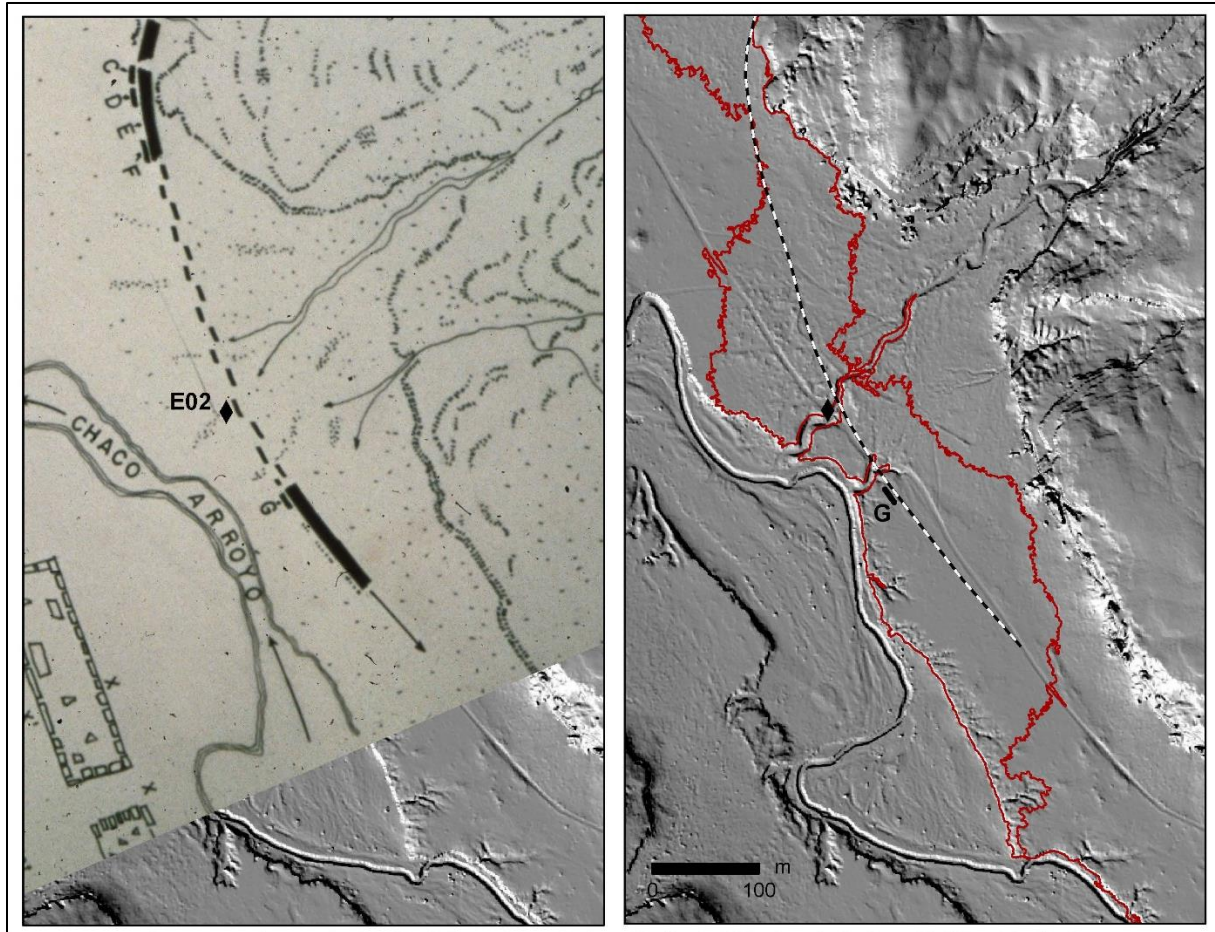
Figure S7.2: The canal cross-section uncovered by Op. E02 (black diamond) is on the line of the Gordon Vivian hypothesized canal (left figure) feeding from Escavada Wash. The lidar-derived topography (right figure) for this area suggests other canals (not shown)—a hydrologically plausible canal between contour lines 1856 m and 1854 m which could feed from the un-incised, ancient version of Chaco Wash and a possible second canal traversing along a recently disused modern road. Figure created by the authors.
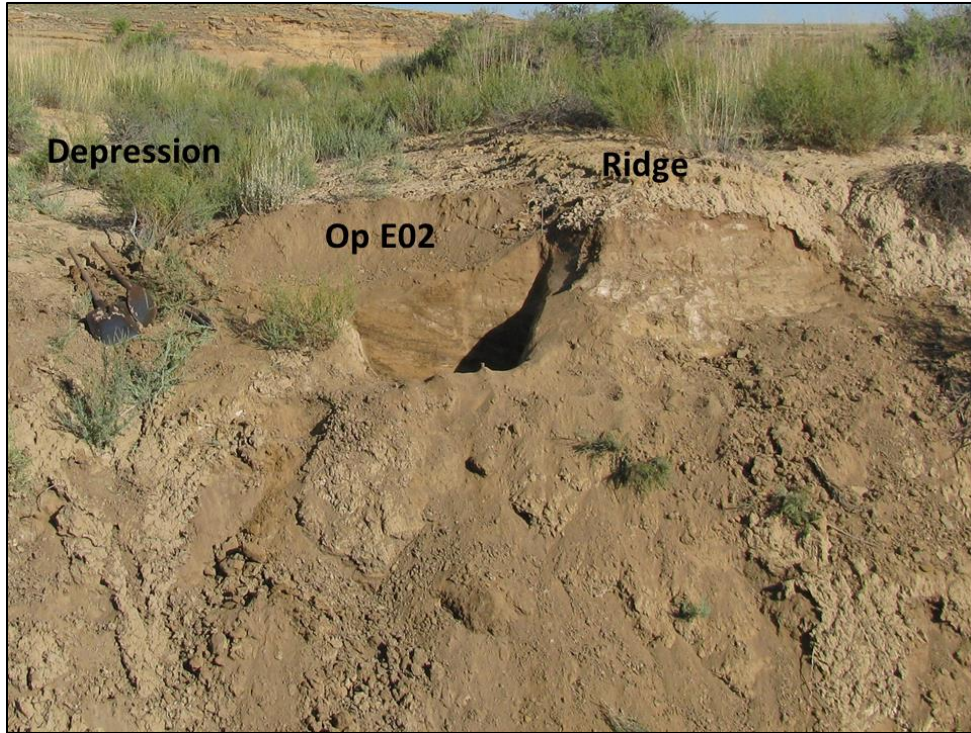
Figure S7.3: The cut-bank along the down-canyon side of Rincon 5N showing a depression which may have held an ancient canal, later used for a wagon trail along with a smaller canal perched on a ridge, our Op. E02. Figure created by the authors.
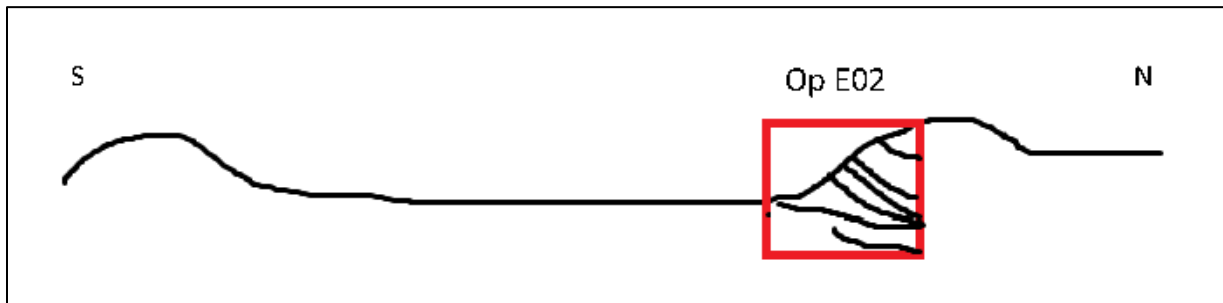

Figure S7.4: A schematic sketch representation of the E02 area. The red box outlines the area of the profile photograph and drawing (Figure 8). Figure created by the authors.

Supplementary Materials 8: Roberts' Great House

During the summers of 2013 and 2014, a crew led by Dr. Adam S. Watson (American Museum of Natural History) mapped and excavated in the site area of Roberts' Great House (RGH) (29SJ2384). RGH is located at the east end of Chaco Canyon National Historical Park, across the Chaco Wash from the McElmo great house of Wijiji. An adjacent, active arroyo channel threatens the site, having already destroyed portions of the northwest and northeast edges of the pueblo. Originally excavated and recorded by Frank H. H. Roberts in 1926 while working for the National Geographic Expedition at Pueblo Bonito with Neil Judd (Roberts 1929; Lister & Lister 1981: 240), fieldwork in 2013 and 2014 sought to assess his conclusions about the now threatened site.

Recent research confirms Roberts' (1929) initial hypothesis that the great house was never completed or occupied (Watson *et al.* 2014, 2015). Few artifacts were encountered and no clearly defined occupation surfaces were identified. Despite the lack of habitation, walls standing a few courses high outline a footprint markedly similar in size and shape to that of nearby Wijiji (Figure S8.1). Wall segments are visible in several places, exposed by arroyo encroachment, and a roughly 1-m portion was uncovered in an excavation unit in 2014. This wall segment found in Study Unit 300 was covered by a meter of alluvial and aeolian sediments, demonstrating the dynamic environmental setting. Additionally, a portion of Roberts' original excavation trench was revealed in profile following the edge of the wall courses.

Dr. Lewis Owen (University of Cincinnati) removed four samples for OSL dating from the two excavation units in 2014: Study Unit 300 and Study Unit 400. The ages are presented in S3 and illustrated here. The OSL ages in Study Unit 300 are transposed (Figure S8.2); an age of 1100±200 BC was located roughly 15 cm higher than the other OSL sample from this unit. The second OSL sample produced an age of AD 1000±40. This sample was taken about 25cm above the top of the wall courses and 85cm below the modern ground surface. Relative to the position of the architecture, and the second OSL sample, the OSL age of 1100±200 BC is inconsistent with its stratigraphic context. Excavation at this site in the 1920s by Roberts might have disturbed the sediment near the surface at this location, incorporating sediment from older deposits and resulting in the older OSL age. Alternatively, the old age might be due to partial bleaching of the sediment, which could have occurred if the sediment was transported and

deposited at night, or in a single high-energy fluvial event in which the water was cloudy with a very thick sediment load; however, this seems less likely given the sound stratigraphic coherence of the other OSL ages in our studies. The second age (AD 1100±40) fits well within expectations given the underlying architecture, but indicates an active environmental setting as deposition over the wall courses occurred rapidly. Substantial accumulation of deposits is also indicated by the complete infilling of Roberts' trench and the current ground surface level.

The two OSL samples removed from Study Unit 400 produced ages of AD 1100±100 and AD 1400±30 in the expected stratigraphic sequence. Twenty-five cm of sediment separate the ages (Figure S8.3), indicating a significant accumulation of deposits in ~300 years. An additional 50 cm of fill, having accumulated in the past ~550 years, separate the higher sample from the surface. Ceramics dating to a range of periods were found in this unit, likely washed in from earlier sites farther up the rincon or on the mesa top. Together, the OSL ages and location of the wall courses in these study units suggest that ground surface during Chaco occupation was nearly a meter below the modern ground surface.

References

LISTER, R.H. & F.C. LISTER. 1981. *Chaco Canyon: archaeology and archaeologists*. Albuquerque: University of New Mexico Press.

ROBERTS, JR., F.H.H. 1929. *Shabik'eshchee village: a late Basket Maker site in the Chaco Canyon, New Mexico* (Smithsonian Institution Bureau of American Ethnology 92). Washington D.C.: Smithsonian Institution.

WATSON, A.S., A. HOLEMAN, S. FLADD, K. BISHOP, M. CONGER & S. MORROW. 2014. Damage assessment and data recovery at 29SJ 2384, Roberts' Great House July-August 2013. Report prepared for the National Park Service, Chaco Culture National Historical Park.

WATSON, A.S., S. FLADD, K. BISHOP, S. MORROW, M. CONGER, L. GILL, & B. BANKSTON. 2015. In the footsteps of Frank H. H. Roberts: continued explorations at Roberts Great House, Chaco Canyon, New Mexico. Poster presented at the 80th Society for American Archaeology Annual Meeting, San Francisco, CA.
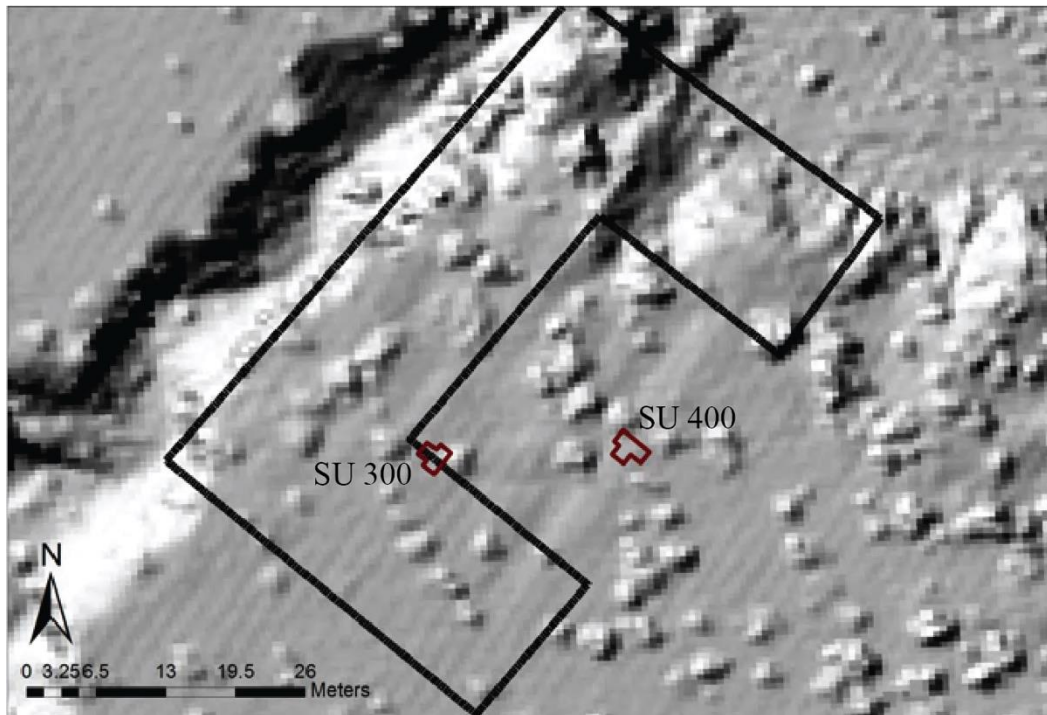
Figures:

Figure S8.1: Estimated extent of Roberts' Great House with 2014 Study Units in red. Figure created by the authors.

Figure S8.2: Study Unit 300 profile with OSL sample locations/ages. Numbers next to OSL ages refer to Chaco 2014-XX in S3.
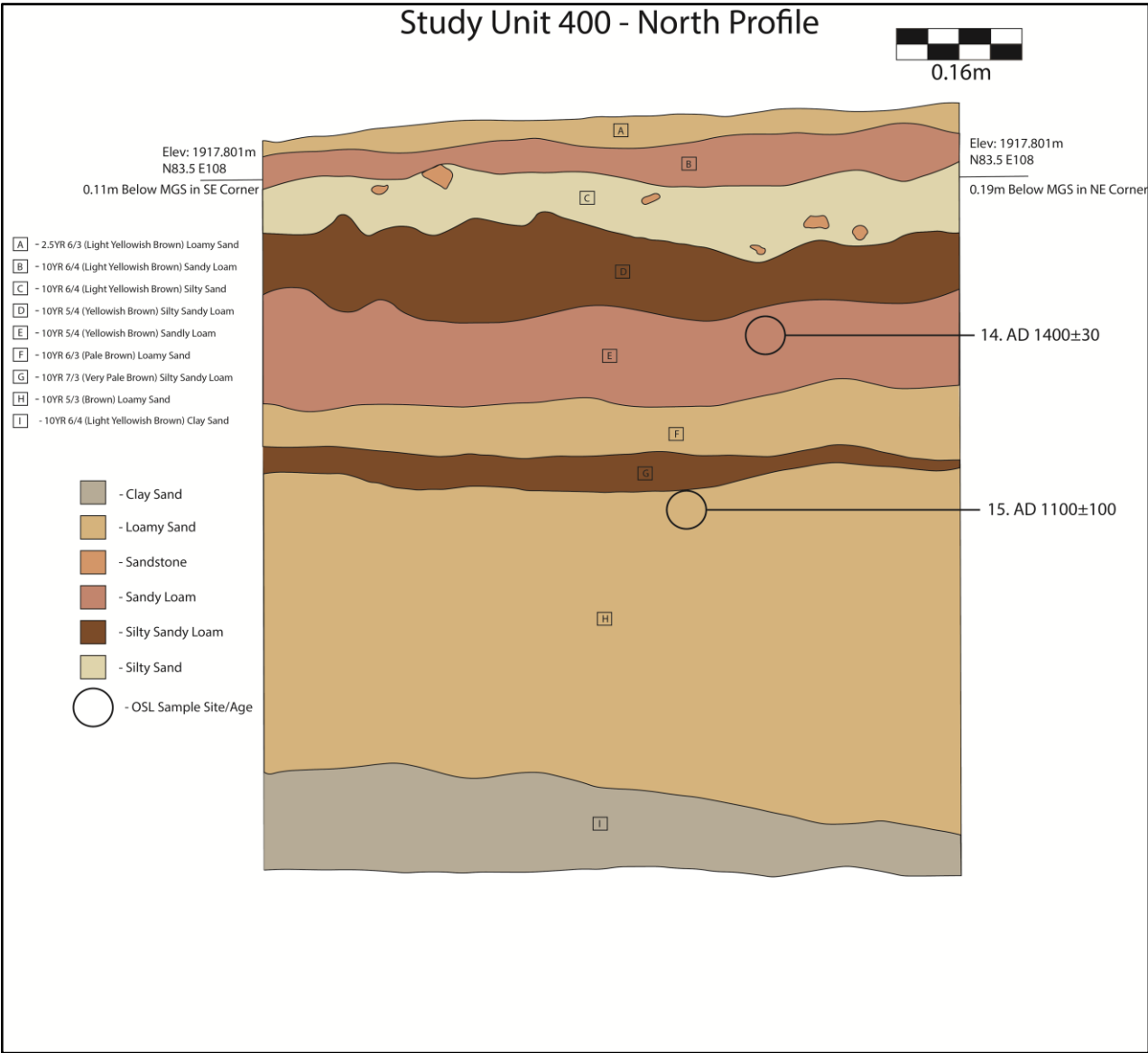
Figure created by the authors.

Figure S8.3: Study Unit 400 profile with OSL sample sites/ages. Numbers next to OSL ages refer to Chaco 2014-XX in S3. Figure created by the authors.